RICE UNIVERSITY

AN APPLICATION OF CORRELATION DETECTION TO THE TIME OF FLIGHT SPECTROSCOPY OF PARTICLE FLUXES

by

William Henry Dragoset, Jr.

A THESIS SUBMITTED
IN PARTIAL FULFILLMENT OF THE
REQUIREMENTS FOR THE DEGREE OF

Master of Arts

Thesis Director's Signature:

Houston, Texas

(April, 1975)

ABSTRACT

An Application of Correlation Detection to the Time of Flight Spectroscopy of Particle Fluxes

by

William Henry Dragoset, Jr.

Linear signal theory analysis has been applied to the problem of finding the time of flight spectra of random and pseudo-random particle fluxes. The results indicate that by employing the methods of correlation detection with suitable particle detectors, significant improvement in the time resolution in some cases and elimination of the pile-up problems of standard particle-by-particle TOF spectroscopy techniques can be achieved. Two different systems based on using correlation detection have been proposed for use with the time coherent LAMPF accelerator beams. One of these, a high speed camera, has been tested at LAMPF. The results of this test are presented. The second system, a method utilizing RF technology, has not been tested.

ACKNOWLEDGEMENTS

The author wishes to express his gratitude to Professor G. C. Phillips for suggesting and supporting this research project and for many useful ideas and discussions during its course.

The contributions of the following to the Imacon camera experiment are sincerely appreciated: Dr. D. Werbeck and Mr. J. Sherwood of LAMPF for their work with the Test Channel beam, the Hadland Company personnel and representatives for their technical assistance, Mr. J. Windish for his construction work, and especially Dr. T. R. Witten for his invaluable assistance in performing the experiment.

The author is indebted to Rice University and the AEC for financial support during this work.

The excellent typing job of the final manuscript was done by Tanya Scheible.

Finally, the author would like to thank his parents for always encouraging his educational advancement and his wife, Mary, for her companionship during the past year.

TABLE OF CONTENTS

I: INTRODUCTION

A: Time of Flight Spectroscopy

A kinematically complete description of a nuclear scattering event requires that a set of parameters be measured that is sufficient to find the momentum of, and unambiguously identify, each of the particles involved in the collision. For example, in pion scattering from a nucleus such as C^{12}, which has its first excited state at 4.4 Mev, the final state of the nucleus is not observable. Consequently, the energy of the scattered pions must be determined in order to separate the elastic and inelastic events. When this experiment is actually performed not all of the scattering events observed are due to incident pions. This is so because an accelerator beam providing pions also contains electrons, protons, and muons.[1] Thus, the identity of each incident particle associated with a particular scattering event must be determined. If absolute cross sections are desired the total incident pion flux, i.e., the beam purity, must also be measured. All of these measurements can be achieved by finding the velocities of the incident and scattered particles.

The experimental technique of measuring the particle velocities in a nuclear scattering experiment is called

time of flight (abbreviated TOF) spectroscopy. The result of a TOF measurement on a particle flux is called its TOF spectrum. This spectrum is usually displayed as a graph of the intensity of the flux versus velocity. In general, there appears to be two antipodal methods of finding TOF spectra. The first of these, the standard method which is fully discussed in sections B and C below, depends on discretely detecting the passages of single particles and arranging them in a time-ordered sequence. The second method, the subject of this paper, continuously measures the space-time characteristics of the flux and extracts the TOF spectrum by correlation methods.

B: Particle-by-Particle TOF Systems

The particle-by-particle technique determines the velocity of a particle by measuring the time during which it travels a known distance. A block diagram of a simple TOF system is shown in Figure 1. A particle passing through one of the detectors produces a pulse which is sensed by the time pick-off unit (TPO). The TPO produces a shaped, logic-level, timing signal. When the time to amplitude converter (TAC) receives a pair of timing signals it produces a single pulse whose amplitude is proportional to the time difference between the signals. As a particle flux

Figure 1: A simple particle-by-particle TOF system. The time of flight of the particle flux is displayed by the multi-channel analyzer as the number of counts versus channel number. The channel number scale is linearly related to time scale.

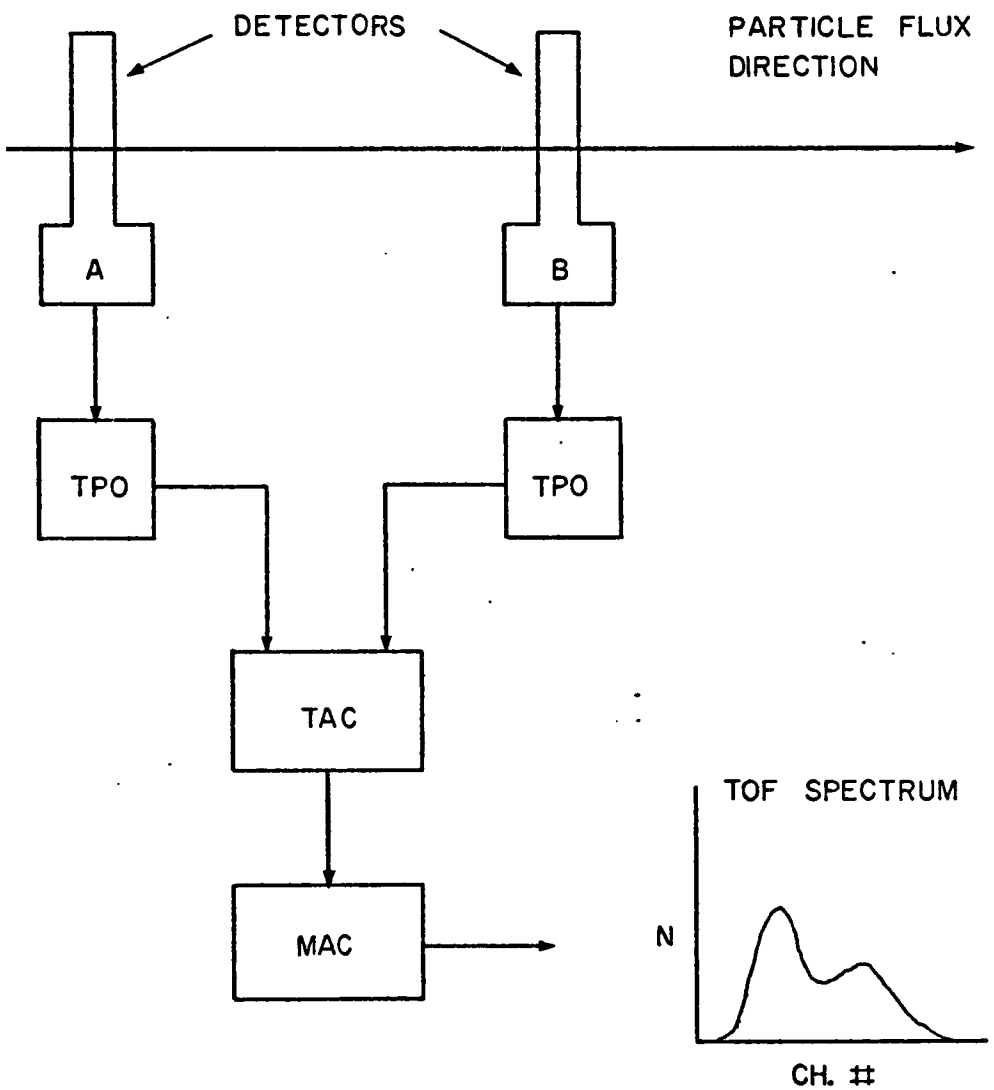
DETECTORS
PARTICLE FLUX DIRECTION
A
B
TPO
TPO
TAC
MAC
TOF SPECTRUM
N
CH. #

passes through the detectors the series of pulses produced by the TAC is stored digitally in a multi-channel analyzer (MCA). Quite often, experiments are done using a pulsed accelerator beam. In this case, one of the TAC inputs may be provided by the accelerator oscillator or by detecting a beam pulse of bunched particles.

The contents of the MCA can be graphically displayed as a plot of the number of pulses observed versus pulse amplitude. Thus, this result is the TOF spectrum of the particle flux. Since the pulse amplitude is linearly related to the time difference, and the distance between the detectors is known, the velocity distribution of the particles in the flux can be determined. Additionally, the amplitudes of the TAC output pulses may be sequentially recorded separately so that the velocity of each particle may be calculated later. Sequentially time-ordered data of this sort is the basic characteristic of particle-by-particle measurements and emphasizes that the measurements are made on a single particle at a time.

C: Limitations of Particle-by-Particle TOF Systems

The performance of an event-by-event TOF system is limited by two factors: time jitter and pile-up. The effects of these factors in any particular experiment depends

on the type of detectors and electronics being used and on the nature and intensity of the particle flux. The particle detector most commonly used for standard TOF applications consists of a light producing material such as a scintillator or Čerenkov radiator optically coupled to a photomultiplier tube. The following discussion uses this type of detector to illustrate the limitations of particle-by-particle TOF systems.

If the relative times of the output pulses of a TPO are plotted for many events it is observed that the time of the output fluctuates about an average value. This phenomena, called time jitter, is due to noise and statistical fluctuations of the transit time of the signal within the detector.[2] The noise in the input to a TPO affects the output because the leading edge of the detector pulse is masked. If the noise were absent, the threshold of the TPO could be set to zero and the slightest non-zero fluctuation of the signal could be used to indicate the occurrence of a pulse. Many ingenious types of time pick-offs have been devised to accurately define the time at which a pulse occurs.[2] There are several sources of transit time fluctuations in light producing particle detectors:[3]

1. Fluctuations in the duration of the light production,

2. Time spread of the light as it travels to the photocathode, and
3. Fluctuations in the electron transit time within the photomultiplier tube.

Pile-up occurs when the particle flux is so intense that it becomes difficult to make observations on a single particle without encountering disturbing effects from other particles passing through the system. For example, two pulses arriving too closely together may cause the relative timing of the output of the TPO to be perturbed. Also, if pulses occur too rapidly it is not possible to correctly pair the two outputs from the TPO units. This problem can be especially severe in experiments using pulsed beams because the instantaneous particle current is much higher than the average current.

State of the art TOF systems presently in use have excellent time resolutions in the range of 1.0 to 0.1 nsec.

However, because of its limited time resolution and pile-up problems, the conventional particle-by-particle TOF technique cannot cope with the requirements of some experiments. Experiment 80 at the Los Alamos Meson Physics Facility (LAMPF), which has recently been done by the Rice University - University of Houston Medium Energy Physics Group, is one such experiment.[4] This experiment used the

P^3 pion beam at LAMPF[5] to study the small angle scattering of pions from several different nuclei. The LAMPF beam, which has the time structure shown in Figure 2, has an instantaneous current of about 340 times the average current. Thus, it was found that when the main beam was 10 μamps and the thick A2 production target was used the scintillators used in the experiment could not handle the full P^3 current because of pile-up. Future experiments will have even more severe problems when the main beam current is increased to 100 μamps.[6]

Experiment 80 provides two examples of cases in which the standard TOF technique is marginal or inadequate. Consider, for example, the problem of identifying the muons in the beam. It can easily be shown that the relation between the time resolution, Δt, and the velocity resolution, $\Delta\beta$, for a TOF path of length d is given by

$$\Delta t = (d/c)\ (\Delta\beta/\beta^2). \qquad \text{(I-1)}$$

For a beam momentum of 250 Mev/c, the velocities of the pions and muons are given by $\beta_\pi = .874$ and $\beta_\mu = .922$, respectively. Thus, to distinguish between these two particles by TOF, the velocity resolution required is at least $\Delta\beta = .048$. If a flight path of 3 meters is used the necessary time resolution is $\Delta t = .6$ nsec. This resolution is difficult to achieve and the long flight path would be an

Figure 2: Time structure of the LAMPF accelerator beam. T_1 is the period of the macrostructure, 8.33 msec; τ_1 is the width of a macropulse, 500 μsec T_2 is the period of the microstructure, 5 nsec; and τ_2 is the width of a micropulse, .25 nsec.

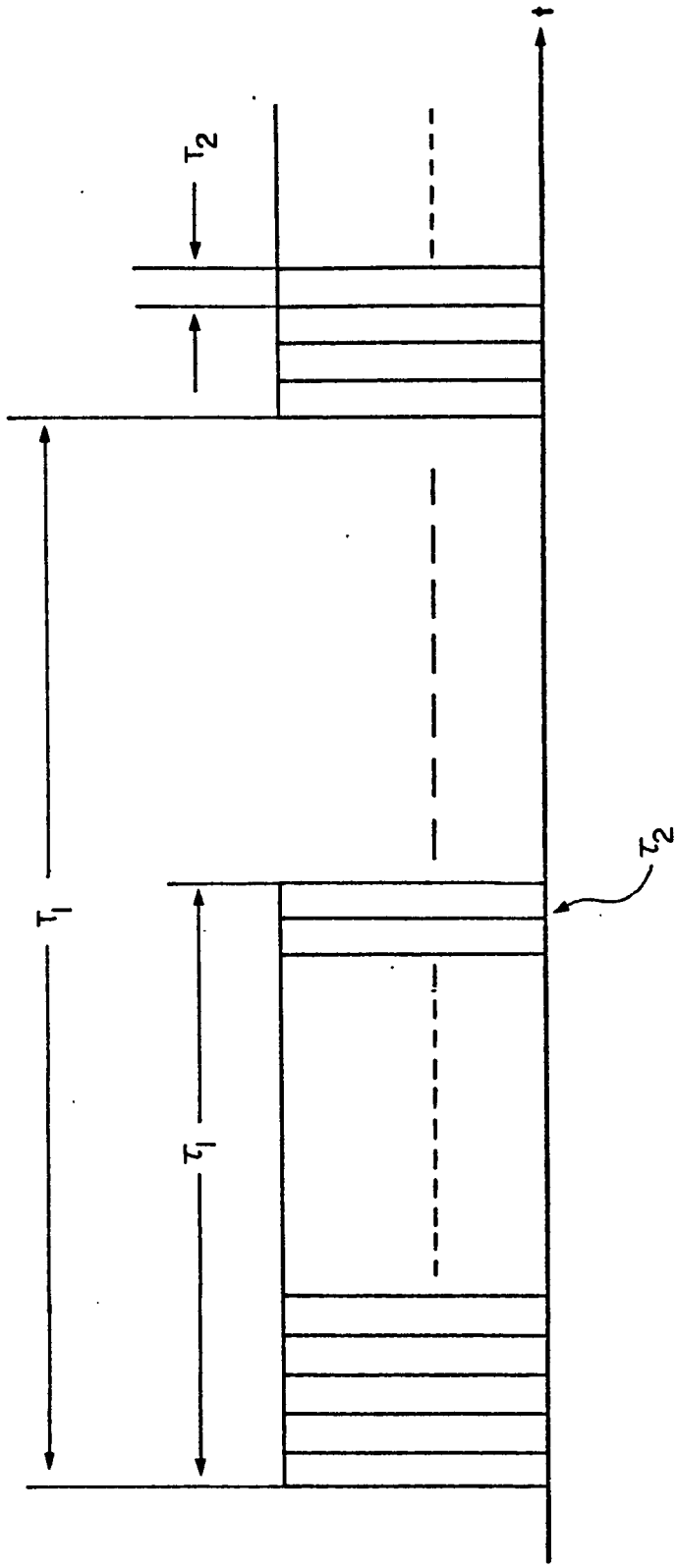
τ2
τ1
τ1
τ2

added inconvenience.

When the pions are scattered from C^{12} the first inelastic pions have 4.4 Mev less energy. At 250 Mev/c this energy amounts to a velocity difference of $\Delta\beta = .004$. Clearly this requires a time resolution ($\Delta t = .05$ nsec) which is not achievable by standard TOF methods.

D: Correlation Detection and Some Uses

As shown in detail in Chapter II, it appears that improved time resolution and elimination of pile-up problems can be achieved by using a technique called correlation detection to find TOF spectra. Basically, correlation detection is a method of comparing two time dependent signals. There are two general ways in which it may be used:

1. If a time dependent signal passes through some kind of system which changes it, correlation detection can be used on the input and output signals to determine the transfer characteristics of the system.
2. If a signal of known characteristics is transmitted through a system it can become distorted and masked by noise. Correlation detection can be used to optimally recover the original signal.

Although it has only recently been applied to detection problems in many diverse fields, correlation is not a new technique. Among its more recent applications are those in the fields of radar detection, radio astronomy, seismology, communications, and thermal neutron spectroscopy.

Probably the first extensive use of correlation techniques was in optical interferometry. This is a method of studying light sources by allowing two images of a source to additively interfere. When the path length of one of the images is altered the intensity of the combined images varies. From this intensity variation Fourier analysis can be used to find the spectral composition of the source. Similar procedures are used to measure the size and distance of remote objects such as stars.[7]

Radar detection offers an excellent example of both uses of correlation detection. In the general problem of radar detection a known series of RF pulses is transmitted into a field of moving objects. The echoes from these objects are frequency shifted due to the Doppler effect and are also masked by noise. In the radar receiver correlation is used not only to improve the signal to noise ratio but also to detect the frequency shifts and thus the velocities of the moving objects.[8]

Another example of correlation detection is found in

the field of seismology. A typical seismological experiment consists of setting off shock waves at many points on the earth's surface and recording, as a function of time, the shock waves reaching several different points. These waves reaching a detection point are a sum of waves traveling directly beneath the surface and waves reflecting upwards from the different rock layers below. The velocity of these waves depends on the elasticity of the material through which they are passing. By recording the shock wave patterns at several points, correlation can be used to separate the meaningful components from the complex noise field and allow a model of the subsurface rock layers to be visualized.[9]

The most extensive use of correlation detection occurs in the fields of communication and information theory. A multitude of problems such as: optimizing the signal to noise ratio of broadcasts, improving radio reception, optimizing filters, and eliminating errors in coded transmissions, have been successfully solved by starting with correlation methods.[10-13]

Correlation detection has been used by Gompf, et. al.[14-15] to find the TOF spectra of thermal neutron beams. This was done by artificially "chopping" the beam before the scattering target with slotted, neutron-absorbing, spinning

wheels. By measuring the neutron current downstream of the target and knowing the chopping function Gompf was able to use correlation procedures to extract the TOF spectrum. Two advantages of the system were the elimination of pile-up problems and the automatic cancelling of detected signals due to background neutrons. Furthermore, it was found that the statistical error in the TOF spectra could be minimized by choosing the correct chopping function.

E: Goals of Research

The major goal of this research work was to demonstrate the feasibility of applying correlation techniques to the problem of finding TOF spectra in general. Of special interest were the applications of this method to experimental conditions for which standard particle-by-particle TOF spectroscopy is useless. An outline of the contents of the following chapters is given here.

In Chapter II it is demonstrated that by treating particle fluxes as time-varying signals, the TOF spectra can be found using correlation detection. The general types of particle detectors necessary to achieve the desired results are discussed. It is shown why correlation detection can improve time resolution. Chapter III describes a high speed camera system which was designed for use at LAMPF. The

results of the test of this system are given and discussed. The theory of Chapter II is used to demonstrate how the camera gives better time resolution.

Chapter IV presents a proposal for a TOF system which detects charged particles by sensing the electromagnetic field of the moving charge. The design of such a system, using correlation detection, for use at LAMPF is presented. An electronic processing system based on RF technology is described.

Finally, Chapter V presents the conclusions drawn from this research and indicates possible directions for future endeavors.

II: THEORY

A large class of physical systems which produce an output dependent on an input can be analyzed by representing the input and output as time varying signals and using a transfer function to describe the action of the system. This approach utilizes a large, standard repertoire of analysis techniques, most of which have been developed for use in the fields of circuit theory, signal theory, and communication theory.[10-13,16,17] These methods have recently been applied to neutron spectroscopy,[14,15,18] seismology,[9] and communications.[13] Appendix A contains a brief review of the basic concepts and formulas of the signal analysis methods used in this paper.

The goal of this section is to apply signal theory to the problem of measuring the TOF spectrum of a particle flux. Section A makes an analogy between a particle flux and a time dependent signal and indicates how the TOF spectrum may be found for a few types of fluxes. Section B discusses the effects of the particle detectors on these measurements in terms of the detector transfer functions and also introduces the complications due to noise. Section C describes a different approach which can be used when a pulsed accelerator beam is available.

A: Particle Fluxes as Time Varying Signals

Consider a tightly bunched pulse of many particles, originally positioned at x = 0 at time t = 0, traveling along an x-axis. If the pulse contains particles of more than one velocity, its shape in time will change as a function of the distance it has traveled. The particle flux at any point, x, which is simply the shape of the pulse at that point, is the TOF spectrum of the original pulse. This situation is analogous to one found in the methods of signal analysis; i.e., the pulse of particles represents an impulse input to a linear system, the TOF path, and the output, the particle flux at x, is the impulse response, h(t,x), of the system (Appendix A). This similarity suggests that particle fluxes may be represented as time dependent signals and that the difference between a flux at two points along its flight path can be represented as the result of sending the corresponding signal through a linear system.

This analogy is strictly true only when the intensity of a flux is such that any small portion of it contains a sufficient number of particles to provide a good statistical representation of the velocity distribution of the flux as a whole. In general, this condition is not found in most accelerator beams. However, in the method for finding TOF spectra discussed below, the contributions of

each portion of a flux to its TOF spectrum are added to obtain the complete spectrum. Thus, from the viewpoint of the experimental result it is immaterial whether a single particle is considered to contribute to the whole spectrum or to just a part of it. This assumption is valid only if the probability of any particular particle having a certain velocity remains constant throughout the course of the experiment; i.e., the velocity distribution must be a stationary random process. Also, of course, this assumption requires that the TOF measurement be continued long enough to achieve statistically meaningful results.

The first case to be considered is that of a completely random particle flux. This implies that the particles occur randomly in time, independent of their velocities. Let the particle flux, f(t), be represented by a chain of impulse functions, each impulse representing a single particle. If the flux at x = 0 is $f_i(t)$ then by equation A19 the flux at any point x is given by

$$f_o(t,x) = \int_{-\infty}^{\infty} h(\nu,x) f_i(t-\nu)\, d\nu. \qquad \text{(II-1)}$$

The crosscorrelation of f_i and f_o is defined (equation A9) by

$$r_{io}(\tau) = \lim_{T\to\infty} (1/2T) \int_{-T}^{T} f_i(t) f_o(t+\tau)\, dt. \qquad \text{(II-2)}$$

By inserting II-1 into II-2

$$r_{io}(\tau) = \int_{-\infty}^{\infty} h(\nu,x) \lim_{T\to\infty}(1/2T) \int_{-T}^{T} f_i(t) f_i(t+\tau-\nu)\,dt\,d\nu, \quad \text{(II-3)}$$

and using equation A10 gives

$$r_{io}(\tau) = \int_{-\infty}^{\infty} h(\nu,x) r_{ii}(\tau-\nu)\,d\nu. \quad \text{(II-4)}$$

Here $r_{ii}(\tau-\nu)$ is the autocorrelation of $f_i(t)$. Thus, the crosscorrelation of a random particle flux at two points along its flight path is the convolution of the TOF spectrum and the autocorrelation at the first point.

Equation II-4 can be solved for $h(\nu,x)$ by first using equation A4 to transform it into a frequency domain representation:

$$R_{io}(\omega) = H(\omega,x) R_{ii}(\omega)$$

$$H(\omega,x) = R_{io}(\omega)/R_{ii}(\omega). \quad \text{(II-5)}$$

Then using equation A3 gives

$$h(t,x) = (1/2\pi) \int_{-\infty}^{\infty} [R_{io}(\omega)/R_{ii}(\omega)] e^{j\omega t} d\omega. \quad \text{(II-6)}$$

Since $f_i(t)$ is a chain of random impulses, $r_{ii}(\tau)$ itself is an impulse and thus $R_{ii}(\omega)$ = a constant, k (equation A14). Then II-6 reduces to

$$h(t,x) = r_{io}(t)/k. \quad \text{(II-7)}$$

This equation states that the TOF spectrum of a random particle flux can be obtained by simply performing the

crosscorrelation of the flux at two points along the flight path. Two comments should be made concerning the use of equations II-2 and II-7 to find the TOF in an actual experiment. First, the limits of integration in equation II-2 actually extend from zero to T where T is the length of time of integration for each τ value. The choice of T is a statistical matter which depends on the intensity of the flux. Secondly, if the detectors measuring the flux produce a unipolar output, the functions $f_i(t)$ and $f_o(t,x)$ will have a non-zero time measure. As a result, $r_{io}(\tau)$ will contain a DC component. This component would have to be subtracted from the computed crosscorrelation before using equation II-7 to obtain the TOF spectrum.

This result can also be easily derived by an intuitive approach. Imagine that a random flux consisting of particles of several different velocities is measured at two points. If the current measured at the first point is delayed by a variable amount and compared to the second current, portions of the two currents will appear equal whenever the delay is such that the portions due to the same velocity reach the comparator simultaneously. When this occurs, the two currents are partially correlated and the delay for which this happens is the TOF of that portion of the flux.

In an actual experiment the functions $f_i(t)$ and $f_o(t,x)$ are the outputs of particle detectors and will not be representable by impulse functions. The effect of the detectors on equation II-6 is considered in section B.

With some careful reservations, equation II-6 can be useful for finding TOF spectra of fluxes which contain time coherent components. The autocorrelation of a function of period T is given by

$$r_{ii}(\tau) = (1/2T) \int_{-T}^{T} f_i(t) f_i(t+\tau)\, dt \qquad \text{(II-8)}$$

and has the same periodicity as the function. However, within the periodic framework of the flux the occurrence of particles is still random. For this reason $r_{ii}(\tau)$ will be greatest when $-T/2<\tau<T/2$. The amount of correlation that occurs outside of this range depends on the intensity of the flux. For example, consider a particle flux which has a 50% probability of having a particle occur exactly at each nT second. Then equation II-8 will give $r_{ii}(\tau = \pm nT)$ on the average equal to $\frac{1}{4} r_{ii}(0)$. Since a single period of most periodic fluxes does not contain a sufficient number of particles to produce good statistics, the integration in equation II-8 is actually carried out for a large number of periods.

If $f_i(t)$ of a periodic flux is observed at some point

along the x-axis other than at x = 0, the velocity of a particle will depend on when within a period T it is observed. This destroys the random property of the flux and will result in extra components in the autocorrelation of $f_i(t)$. Thus, $f_i(t)$ must be measured only at x = 0; i.e., at the point for which the probability of a particle having a certain velocity is truly random.

If the time structure of a periodic flux and the velocity distribution of the particles in the flux are such that some of the particles observed in the $n^{\underline{th}}$ period of $f_o(t)$ originated in the $n^{\underline{th}}$ - 1 period of $f_i(t)$ then ambiguous results can occur. This is so because these particles could correlate with particles in the $n^{\underline{th}}$ period of $f_o(t)$ and hence would appear as "fast" rather than "slow" particles. This problem likewise depends on the intensity of the flux; i.e., if there is only a slight correlation between adjacent periods of $f_i(t)$ then there will be little chance of these slow particles correlating with the following period. If they do, however, this method cannot be used. This same effect occurs in particle-by-particle TOF spectroscopy much more seriously and is called "wrap around." That is, when a particle is detected it cannot be identified as either a fast particle from the $n^{\underline{th}}$ pulse or a slow particle from the $n^{\underline{th}}$ - 1 pulse.

In general then, equation II-6 can be applied to periodic fluxes only if:

1. $f_i(t)$ is measured at $x = 0$,
2. the TOF of the slowest particles for a particular $f_o(t,x)$ does not exceed the length of one period, and
3. τ is varied only over the range of one period.

For low intensity fluxes all three conditions can be relaxed. Fortunately, a different method of treating high intensity pulsed beams is available. This is discussed in section C.

B: Particle Detectors and Noise

Figure 3 shows a schematic diagram of a detection system that can be used to implement the correlation method described above. The two detectors which are used to detect the particle currents are represented by their transfer functions, $D_1(\omega)$ and $D_2(\omega)$. The outputs of these detectors, $g_i(t)$ and $g_o(t)$, will, in general, depend on the particle fluxes, the transfer functions, and the noise, $N(t)$. The total noise is a combination of noise produced within the detectors and noise present in the particle fluxes. In the figure, the noise is shown as an additional input to the detectors. The detector outputs are correlated to pro-

Figure 3: A system for using correlation techniques to find the TOF spectrum of a particle flux. $d_1(t)$ and $d_2(t)$ are the impulse responses of the detectors.

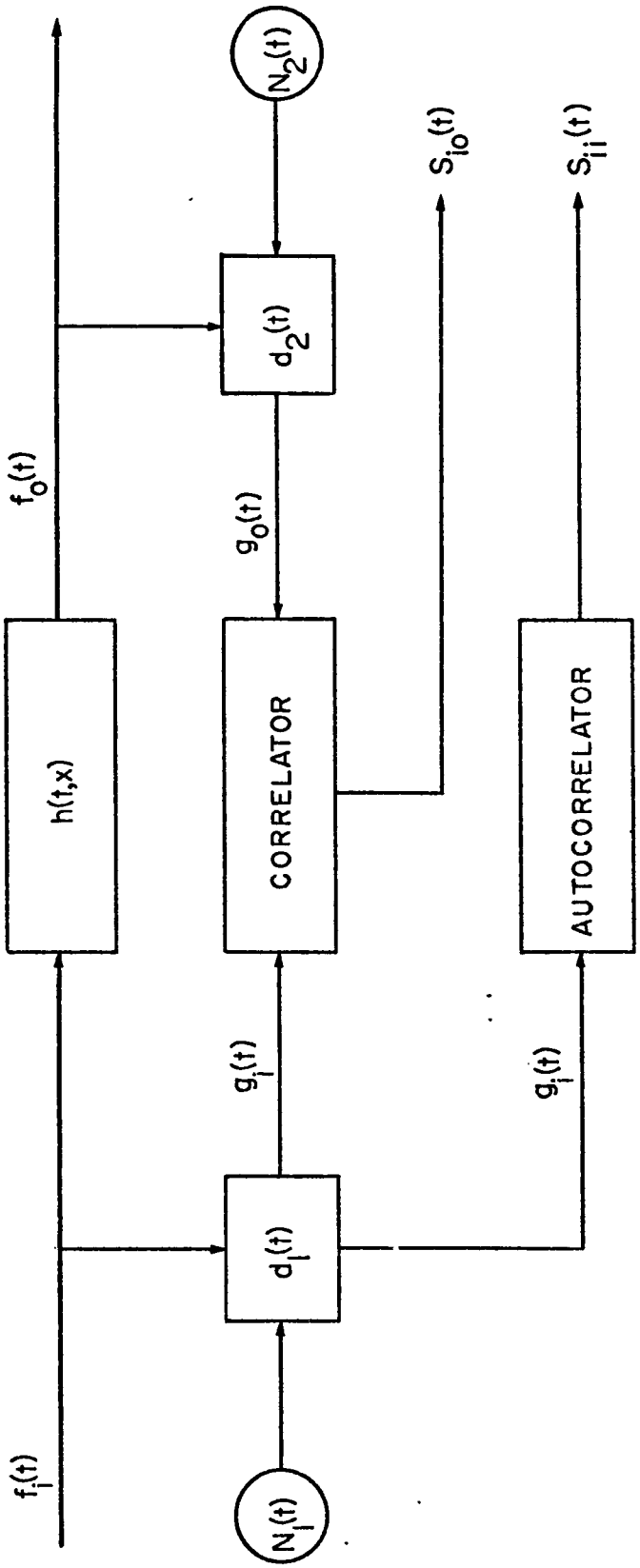
$N_2(t)$
$S_{io}(t)$
$S_{ii}(t)$
$d_2(t)$
$f_o(t)$
$g_o(t)$
h(t,x)
CORRELATOR
AUTOCORRELATOR
$g_i(t)$
$g_i(t)$
$d_1(t)$
$f_i(t)$
$N_1(t)$

duce the functions $s_{ii}(\tau)$ and $s_{io}(\tau)$. These two functions will not be identical to the $r_{ii}(\tau)$ and $r_{io}(\tau)$ correlations in equation II-6. The effects of the noise will initially be ignored in order to clarify the discussion of the effects of the detector characteristics.

In order to use equation II-6 to find h(t,x) it is necessary to find $r_{io}(\tau)$ and $r_{ii}(\tau)$ in terms of $s_{io}(\tau)$ and $s_{ii}(\tau)$. From equation A19

$$\begin{aligned} g_i(t) &= \int_{-\infty}^{\infty} d_1(\nu) f_i(t-\nu)\, d\nu \\ g_o(t) &= \int_{-\infty}^{\infty} d_2(\sigma) f_o(t-\sigma)\, d\sigma. \end{aligned} \tag{II-9}$$

But from equation A9

$$s_{io}(\tau) = \lim_{T\to\infty} (1/2T) \int_{-T}^{T} g_i(t) g_o(t+\tau)\, dt. \tag{II-10}$$

So using equations II-9 in equation II-10 gives

$$\begin{aligned} s_{io}(\tau) = \int_{-\infty}^{\infty} d_1(\nu) \int_{-\infty}^{\infty} d_2(\sigma) \lim_{T\to\infty}(1/2T) \int_{-T}^{T} f_i(t-\nu) \\ f_o(t+\tau-\sigma)\, dt\, d\sigma\, d\nu. \end{aligned} \tag{II-11}$$

Substituting $r_{io}(\tau)$ from equation II-2 leaves

$$s_{io}(\tau) = \int_{-\infty}^{\infty} d_1(\nu) \int_{-\infty}^{\infty} d_2(\sigma) r_{io}(\tau+\nu-\sigma)\, d\sigma\, d\nu. \tag{II-12}$$

Let $t = \sigma - \nu$, then

$$s_{io}(\tau) = \int_{-\infty}^{\infty} d_1(\nu) \int_{-\infty}^{\infty} d_2(\nu + t) r_{io}(\tau - t)\, d\nu\, dt. \qquad \text{(II-13)}$$

By reversing the order of integration

$$s_{io}(\tau) = \int_{-\infty}^{\infty} r_{io}(\tau - t) r_{d_1 d_2}(t)\, dt, \qquad \text{(II-14a)}$$

where $r_{d_1 d_2}(t)$, the crosscorrelation of the detector transfer functions, is defined by

$$r_{d_1 d_2}(t) = \int_{-\infty}^{\infty} d_1(\nu) d_2(\nu + t)\, d\nu. \qquad \text{(II-15)}$$

A similar derivation results in

$$s_{ii}(\tau) = \int_{-\infty}^{\infty} r_{ii}(\tau - t) r_{d_1 d_1}(t)\, dt. \qquad \text{(II-14b)}$$

Equation II-14a states that the crosscorrelation actually measured is given by the convolution of the true crosscorrelation and the response crosscorrelation of the detectors. Changing to the frequency domain via equation A4:

$$S_{io}(\omega) = R_{io}(\omega) R_{d_1 d_2}(\omega)$$

$$S_{ii}(\omega) = R_{ii}(\omega) R_{d_1 d_1}(\omega) \qquad \text{(II-16)}$$

It can be shown using equations A4 and II-15 that

$$R_{d_1 d_2}(\omega) = D_1^*(\omega)\, D_2(\omega). \qquad \text{(II-17)}$$

Finally, h(t,x) is given by:

$$h(t,x) = (1/2\pi) \int_{-\infty}^{\infty} [S_{io}(\omega)/S_{ii}(\omega)]\,d\omega$$

$$= (1/2\pi) \int_{-\infty}^{\infty} [R_{io}(\omega)/R_{ii}(\omega)]\,[D_2(\omega)/D_1(\omega)]\,d\omega. \qquad \text{(II-18)}$$

This equation shows that the effect of the detectors is contained in the function $D_2(\omega)/D_1(\omega)$.

From the viewpoint of the macroscopic dimensions of a particle detector, the time it takes a particle to pass a point in space is negligible. An ideal detector, located at position x, should produce an impulse function whenever a particle passes position x. A real detector, however, produces a delayed pulse that has a finite width, Δt. The size of Δt for a particular type of detector depends on the mechanism by which it senses the passage of a particle. For example, Δt for a Čerenkov radiator depends on the thickness of the radiator (Appendix C). As another example, consider a detector which detects the passing electric or magnetic field of a charged particle. The width of this field is given by:[21]

$$\Delta t \sim b/(\gamma v), \qquad \text{(II-19)}$$

where b is the impact parameter and γ is the usual relativistic factor $1/[1 - (v^2/c^2)]^{\frac{1}{2}}$; hence, the width of the detector output depends on the velocity and the position of

the particle relative to the detector. To facilitate the derivation below it will be assumed that over the range of velocities of interest within a particle flux the pulse width of the detector output is constant. Additionally, it will be assumed that the detector output is linear; i.e., the output due to a group of particles is the sum of the single particle outputs.

A simple way of characterizing the response of a particle detector is to treat it as a low pass filter (Appendix A). The advantage offered by this is that just a single parameter, the cut-off frequency, ω_c, can be used to describe the transfer function of the detector. From Appendix A, $\omega_c \approx \pi/\Delta t$. This will not allow any exact results to be calculated because the shape of the detector response will not, in general, be identical to the shape of a low pass filter's impulse response and the dependence of shape on particle velocity is being ignored. However, this treatment will allow approximate results concerning the time resolution and the pile-up to be derived. Of course, a particle detector is not really a filter in the electrical network sense because it cannot actually be tested by applying inputs of various frequencies. The low pass filter treatment is merely a convenient analogy.

If $D(\omega)$ is the transfer function of a low pass filter

then using equation A20 in equation II-17 leads to

$$R_{dd}(\omega) = \begin{cases} A^2 & \omega \leq \omega_c \\ 0 & \omega > \omega_c \end{cases} \qquad \text{(II-20)}$$

if the detectors are identical. Here A is a constant describing the amplitude of the detector output. Substituting into equation II-16 gives

$$S_{io}(\omega) \text{ or } S_{ii}(\omega) = \begin{cases} A^2 R_{io}(\omega) \text{ or } R_{ii}(\omega) \\ 0 \end{cases}, \qquad \text{(II-21)}$$

or, using equation II-18,

$$h(t,x) = (1/2\pi) \int_{-\omega_c}^{\omega_c} [S_{io}(\omega)/S_{ii}(\omega)]\, d\omega = (1/2\pi) \int_{-\omega_c}^{\omega_c} [R_{io}(\omega)/ R_{ii}(\omega)]\, e^{j\omega t} d\omega. \qquad \text{(II-22)}$$

This derivation shows the important result that if the two detectors are identical then their only effect upon the TOF spectrum, h(t,x), is to limit its bandwidth. That is, the actual shape of the transfer functions, D(ω), will not affect the result. The time resolution of the system depends directly on the bandwidth of the function h(t,x). This can be seen most easily by considering a flux with all particles having the same velocity and by letting $R_{ii}(\omega)$ be a constant, k_1, as was done in equation II-7. Under these conditions $r_{ii}(\tau)$ should be an impulse function located at $\tau = x/v$. Then from equation A5, $R_{io}(\omega) = k_1 e^{-j\omega x/v}$ and from

equation A21

$$h(t,x) = (k_1/k_1)(1/2\pi)\int_{-\omega_c}^{\omega_c} e^{j\omega(t-x/v)}\,d\omega$$

$$= 1/\pi\ [\sin\omega_c(t-x/v)]\ /(t-x/v). \qquad \text{(II-24)}$$

The width of this pulse is $\Delta t' \approx 1/2f_c$ or $\Delta t' = \pi/\omega_c$. Or since $\omega_c \approx \pi/\Delta t$,

$$\Delta t' \approx \Delta t. \qquad \text{(II-25)}$$

Thus, the time resolution of the correlation system shown in Figure 3 is approximately equal to the width, in time, of the pulses produced by the detectors when a single particle passes through.

The advantages and disadvantages of this system in terms of time resolution and pile-up are discussed after the following discussion of noise effects.

The noise in the correlation system of Figure 3 is a stationary random process. This means that it is independent of any other signals present in the system. As a result, the noise will not correlate with $g_1(t)$ or $g_o(t)$. The contribution of the noise to $s_{io}(\tau)$ can be calculated as follows:

$$g_i'(t) = \int_{-\infty}^{\infty} d_1(\nu)[f_i(t-\nu) + N_1(t-\nu)]\,d\nu$$

$$g_o'(t) = \int_{-\infty}^{\infty} d_2(\sigma)[f_o(t-\sigma) + N_2(t-\sigma)]\,d\sigma. \qquad \text{(II-26)}$$

or using equations II-9:

$$g_i'(t) = g_i(t) + \int_{-\infty}^{\infty} d_1(\nu) N_1(t-\nu)\, d\nu$$

$$g_o'(t) = g_o(t) + \int_{-\infty}^{\infty} d_2(\sigma) N_2(t-\sigma)\, d\sigma. \qquad \text{(II-27)}$$

This gives

$$s_{io}'(\tau) = \lim_{T\to\infty}(1/2T) \int_{-T}^{T} \Big\{ g_i(t) g_o(t+\tau) + g_i(t) \int_{-\infty}^{\infty} d_2(\sigma)$$

$$N_2(t+\tau-\sigma)\, d\sigma + g_o(t+\tau) \int_{-\infty}^{\infty} d_1(\nu) N_1(t-\nu)\, d\nu \qquad \text{(II-28)}$$

$$+ \int_{-\infty}^{\infty} d_1(\nu) N_1(t-\nu)\, d\nu \int_{-\infty}^{\infty} d_2(\sigma) N_2(t+\tau-\sigma)\, d\sigma \Big\} dt,$$

or

$$s_{io}'(\tau) = s_{io}(\tau) + \int_{-\infty}^{\infty} d_2(\sigma) \lim_{T\to\infty}(1/2T) \int_{-T}^{T} g_1(t) N_2(t+\tau+\sigma)\, dt\, d\sigma$$

$$+ \int_{-\infty}^{\infty} d_1(\nu) \lim_{T\to\infty}(1/2T) \int_{-T}^{T} g_o(t+\tau) N_1(t-\nu)\, dt\, d\nu$$

$$+ \int_{-\infty}^{\infty} d_1(\nu) \int_{-\infty}^{\infty} d_2(\sigma) \lim_{T\to\infty}(1/2T) \int_{-T}^{T} N_1(t-\nu) N_2(t+\tau-\sigma)$$

$$dt\, d\sigma\, d\nu. \qquad \text{(II-29)}$$

However, the last three terms each add at most a constant because the functions in the time integrals are uncorrelated. As a result,

$$s_{io}'(\tau) = s_{io}(\tau) + \text{constant}. \qquad \text{(II-30)}$$

A similar result can be derived for $s_{ii}'(\tau)$. In an actual experiment the constants would be subtracted by the correlators. Thus, the noise present in the system does not affect the measurement of the TOF spectrum.

The major advantage of this correlation system is its ability to handle high flux rates. Since the only limitation placed on the detectors was that they operate linearly, there is no problem associated with pile-up unless the dynamic range of the detectors is exceeded. On the other hand, the time resolution using a particular type of detector will not be as good for the correlation system as it would be for a particle-by-particle system. This is so because the time resolution of the correlation system depends on the detector pulse width while in the particle-by-particle system the timing depends on only the leading edge of the pulse. However, since the noise in the correlation system does not affect the measurement, it may be possible to design low gain detectors with small pulse widths that could not be used in a standard system.

The major disadvantage of all correlation methods is the loss of single particle identification. This is especially serious in experiments which require single event parameters to calculate unmeasured results. This drawback could possibly be surmounted in some experiments by using

more complicated correlators. For example, experiments detecting coincidences between scattered particles could use a system of gated correlators so that the TOF spectrum would contain only contributions from the particles of interest. Another serious disadvantage is the problems encountered by this method with time coherent fluxes of high intensity, high fundamental frequency, or both. The following section describes an alternate method of correlation which can be used for these cases.

C: Correlation Detection for Periodic Fluxes

As was mentioned in section A above, one of the characteristics of periodic particle fluxes is that a correlation exists between the particle velocities and their phases with respect to the fundamental frequency of the flux. The phase of each velocity component depends on the velocity and the position x along the flux axis. If a velocity component of a periodic flux of fundamental frequency ω_o has the phase angle $\varphi = 0$ at $x = 0$ at $t = 0$, then at point x

$$\varphi = \omega_o x/v = \omega_o t_d. \qquad \text{(II-31)}$$

Here t_d is the time of flight for the particles with the velocity v to travel the distance x. Equation II-31 suggests that if the phase components in a periodic flux can be measured then the TOF spectrum is known.

If the phase of a velocity component can be measured with resolution $\Delta\varphi$ then the time resolution is

$$\Delta t = \Delta\varphi/\omega_o . \qquad \text{(II-32)}$$

For example, if $\Delta\varphi$ could be measured to within 1° for a beam at LAMPF, which has $\omega_o = 4\pi \times 10^8$ rad/sec, then Δt = 15psec. This remarkable result is an improvement by a factor of almost two orders of magnitude over the standard particle-by-particle TOF methods.

A periodic flux, f(t,x), can be described by

$$f(t,x) = \sum_v f_v(t,x) = \sum_v \sum_n F_v(n) e^{jn\omega_o(t-x/v)} . \qquad \text{(II-33)}$$

If the velocity destribution is continuous then $\sum_v$ is replaced by $\int dv$ and $F_v(n)$ becomes a continuous function of v. In the notation used above $F_v(n)$ is a complex number which depends on the amplitude, A_n, and the phase, φ_n, of the n^{th} component of the sum. In reality, equation II-33 cannot actually describe a particle flux because the number of particles in each period randomly fluctuates about some average value. However, as was done in section A, it may be argued that since the experimental results will be found by performing an integration over many periods, f(t,x) can be treated as the average flux without affecting the final results.

It will be assumed in the following discussions that a

"sync" signal, $\cos\omega_o t$, that is phase synchronized to the particle flux is available. This signal would usually come from the oscillator which controls the frequency of the accelerator producing the flux.

For a given value of x the periodic structure of the flux can be found by summing the particle current of each period over a large number of periods. The role of the sync signal is to properly define each period to ensure that for a given t the points added are f(t), f(t+T), f(t+2T), etc., where T is the period. This process may be mathematically described as follows.

Consider a periodic chain of impulse functions defined by the function $m(\tau)$ where

$$m(\tau) = \sum_{\ell} \delta(\tau - \ell T). \qquad \text{(II-34)}$$

By letting $\tau = t-s$, then

$$g(s,x_o) = \int_{-\infty}^{\infty} f(t,x_o)m(t-s)dt \qquad \text{(II-35)}$$

where $g(s,x_o)$ is the desired result and s varies from 0 to T. The function m(t-s) can be visualized as a periodic chain of "windows" where the phase of the windows depends on s. The actual rate at which s is varied depends on the detection apparatus and does not affect the outcome of the measurement as long as the data collection time is constant for each value of s throughout the period T and the average

$f(t,x)$ remains constant. If s is varied so that the window moves with $f(t,x_o)$ through each period then the detection method is known as stroboscoping.[8] The form of equation II-35 illustrates that a correlation detection process is being used.

As in the system discussed previously, the sources of noise in the above detection method are the detector itself and the background particle flux. In this case, however, the background flux may contain time coherent components which are not separable from the desired signal. As is demonstrated in the following argument, the signal to noise ratio for the true noise components can be estimated by statistical considerations.

Assume that within a particular interval of the period T a recurring signal of amplitude A is recorded. In addition to the signal a random noise distribution, N(s), also occurs within each period. Because of its random nature the noise distribution can be characterized only by its mean value, $\overline{N}$, and its standard deviation, σ. After summing over L periods, the signal amplitude will be LA, the mean noise will be $L\overline{N}$, and the standard deviation of the noise will be $\sqrt{L}\,\sigma$.[24] If $L\overline{N}$ (which can be determined by a separate run without the signal present) is subtracted from the distribution, the result will be a distribution consis-

ting of the signal plus the statistical deviations of the noise. Thus, the signal to noise ratio is a measure of the signal amplitude compared to the average statistical deviations of the noise. That is,

$$S/N = L^2A^2/(L\sigma^2) = L(A^2/\sigma^2). \qquad \text{(II-36)}$$

This equation shows that the signal to noise ratio is improved by the number of periods recorded. If the noise amplitude is much greater than the signal amplitude for a single period then A^2/σ^2 will be small. In this case the S/N improvement could be severely limited by the dynamic range of the system (see Chapter III for an example).

If the flux contains a very simple velocity distribution and a reference phase angle can be established then $g(s,x_o)$ of equation II-35 is sufficient to find the TOF spectrum. If the phase of the particles as they emerge from the accelerator is known with respect to $\cos\omega_o t$ then this may be used as a reference with which to compare the phases of the velocity components in $g(s,x_o)$. Equation II-31 can then be used to find the TOF spectrum. In most cases, however, the information contained in $g(s,x_o)$ is not sufficient to give the TOF spectrum. This is so because if the velocity components overlap within the periodic structure there is no way to distinguish then by simply knowing $g(s,x_o)$ at one point. It is very likely that the velocity

components will overlap because periodic accelerators produce particles for a certain length of time in each period. For example, at LAMPF (Figure 2) the pulses occupy approximately 1/20 of the microperiod. Thus, even a flux of only a single velocity will appear to have a distribution (rather than a sharp spike) in $g(s,x_o)$.

A complete knowledge of $g(s,x)$ is sufficient to find the TOF spectrum. This is so because a comparison of $g(s,x)$ for different x positions will show the relative phases of the velocity components shifting. The amount of shift for each component will be dependent on its velocity, and so the velocity distributions can be untangled. Even with $g(s,x)$ completely determined a complicated computer analysis will be necessary to solve the general problem.

Actually, $g(s,x)$ contains some unnecessary information. This is so because only the relative amplitudes and the phases of the velocity components are needed for equation II-31. This implies that the required information about each velocity component is carried by its fundamental frequency compenent, $\cos\omega_o(t-x/v)$. The phases of these components can be detected by correlating the particle flux, $f(t,x)$, with the sync signal:

$$g(x,\tau) = (1/mT)\int_o^{mT} \cos\omega_o(t+\tau)f(t,x)dt. \qquad \text{(II-37)}$$

By using equation II-33

$$g(x,\tau) = \sum_{v}\sum_{n} F_v(n)e^{-jn\omega_o x/v}(1/mT)\int_{o}^{mT}\cos\omega_o(t+\tau)e^{jn\omega_o t}dt. \quad \text{(II-38)}$$

Since the cosine and sine fucntions are orthogonal functions equation II-38 reduces to the form

$$g(x,\tau) = \sum_{v} A_v\cos[\omega_o(x/v+\tau)+\varphi_v]. \quad \text{(II-39)}$$

Here, A_v and φ_v are the amplitude and phase from $F_v(1)$. It is reasonable to assume that for some x = 0 the velocity components are all in phase. At this point φ_v can be set equal to zero.

$$g(x,\tau) = \sum_{v} A_v\cos(\omega_o\tau+\theta_v(x)), \quad \text{(II-40)}$$

where $\theta_v = \omega_o x/v$. This result has a much simpler form than g(s,x) in equation II-35 and consequently, the solution of the TOF spectrum is simpler in the general case (See Appendix B).

Figure 4 shows a simple experimental set-up to measure $g(x,\tau)$. The contributions of the noise to $g(x,\tau)$ is negligible as is seen by the following analysis:

If a random white noise is added to f(x,t) then from equation II-37

$$g'(x,\tau) = g(x,\tau) + (1/mT)\int_{o}^{mT}\cos\omega_o(t+\tau)N(t)dt. \quad \text{(II-41)}$$

Since the noise is white it has a constant power spectrum

Figure 4: A correlation system for periodic fluxes. The sync signal is phase locked to the periodic structure of the flux. $g(x_o,\tau)$ can be analyzed to find the TOF spectrum.

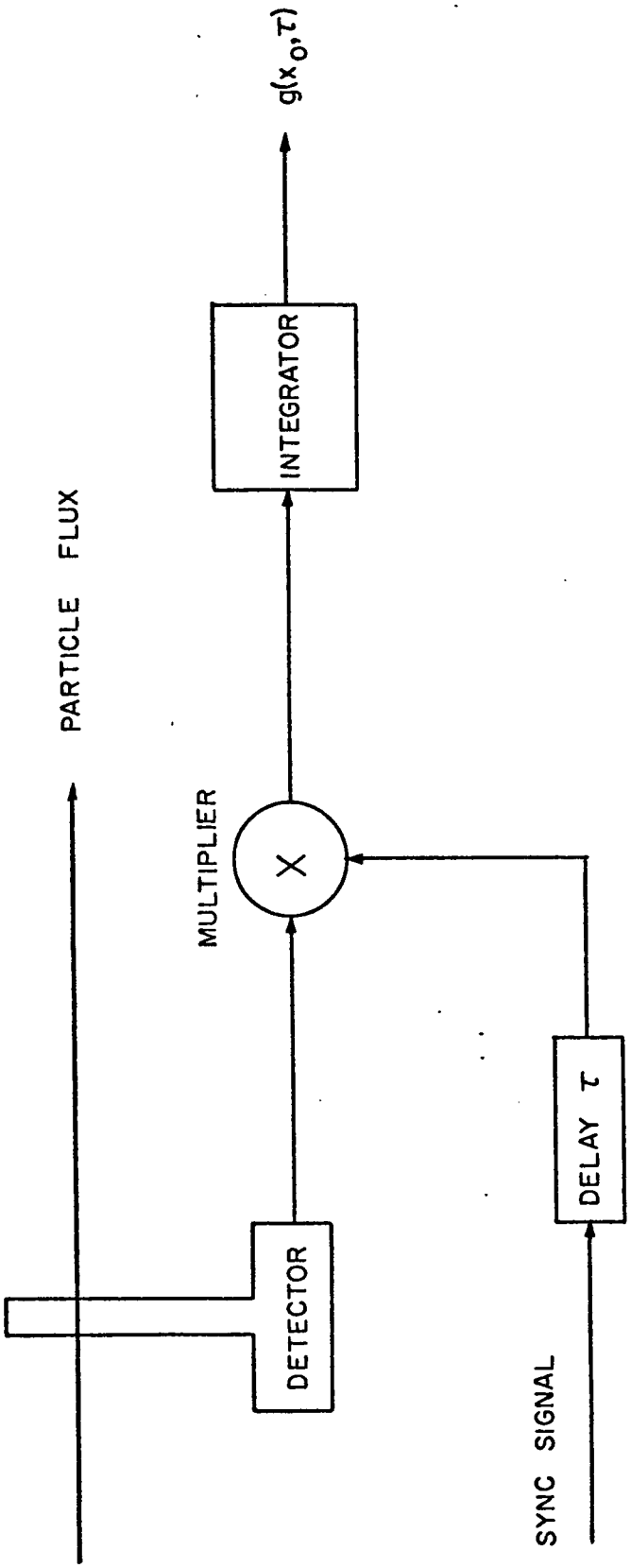
$g(x_0,\tau)$
INTEGRATOR
PARTICLE FLUX
MULTIPLIER
X
DETECTOR
DELAY τ
SYNC SIGNAL

and hence the ω_o component, the only component which can contribute to the integral, will add a negligible factor to $g(x,\tau)$.

Two methods of correlation detection for use with periodic fluxes have been discussed in this section. In lieu of the discussion of specific detection systems based on these methods, in the next two chapters the advantages and disadvantages of these two methods will be covered.

III: THE IMACON CAMERA EXPERIMENT

There are several methods of applying the technique of correlation detection to the TOF spectroscopy of particle fluxes. The two methods described in this chapter and the next were designed for use with the LAMPF accelerator beams which have the time coherent structure shown in Figure 2. Both designs utilized the phase-locked RF accelerator oscillator signal (section C) as the reference correlation signal. Either method could be made compatible with other pulsed beams by adjusting the fundamental frequency for which they were designed.

Any low level signal detector must have acceptable specifications in three categories:

Sensitivity - a measure of the minimum input signal magnitude which produces the desired output level.

Dynamic Range - the range of input levels over which the output suffers no non-linear distortion.

Signal to Noise Ratio - the ratio between the signal output power and the noise power added by the detector.

The criteria necessary in these three categories will be discussed in conjunction with each design in the appropriate section.

A charged particle can be detected by its ability to

produce light in a scintillator or a Čerenkov radiator or by detecting the changing electromagnetic flux caused by the moving charge. The Imacon camera system, which is the subject of this section, is essentially a light detecting system. The system discussed in Chapter IV, which detects the electromagnetic fields of the particles, is merely a proposal. No tests are reported.

A: Description of the Imacon Camera System

The light detecting system used for this experiment was a specially modified version of the Imacon 600 camera produced by John Hadland (Photographic Instrumentation) Ltd. The two major components of this system were a unique image converter tube and an image intensifier. The specifications supplied by the manufacturer are listed in Table I.

A cross sectional view of the image converter tube is shown in Figure 5. An objective lens was used to form an image of the light from the particle detector on the S20 photocathode. A 20kv negative potential with respect to the grounded anode and screen was applied to the cathode. As a result of this potential the optical image was converted into an electron beam which was focused towards the screen. The shutter plates, a feature which was not used in this experiment, were capable of turning the electron

Table I: Manufacturer's Data for Imacon Camera

Transit time spread within image converter tube	2 psec
Phase-locking accuracy within one beam cycle	± 2.5 psec
Image intensifier gain	10^5
Approximate efficiency of photocathode to Čerenkov light	10% - 12%
Photons produced at film plane/ photoelectron	6×10^4
Spot size at film plane for single photoelectron	100_μ diameter
Polaroid 410 film requirement for density change of .5	5×10^8 photons/cm^2
Synchronizing signal amplitude required	2 volts
Size of circular scan	variable to 40mm diameter
Estimated time resolution for spot source	4.5 psec

Figure 5: The Imacon camera image converter tube. Photons incident on the photocathode at the left are converted into an electron beam which is focused and shifted by potentials on the various plates to produce an image on the phosphor screen at right.

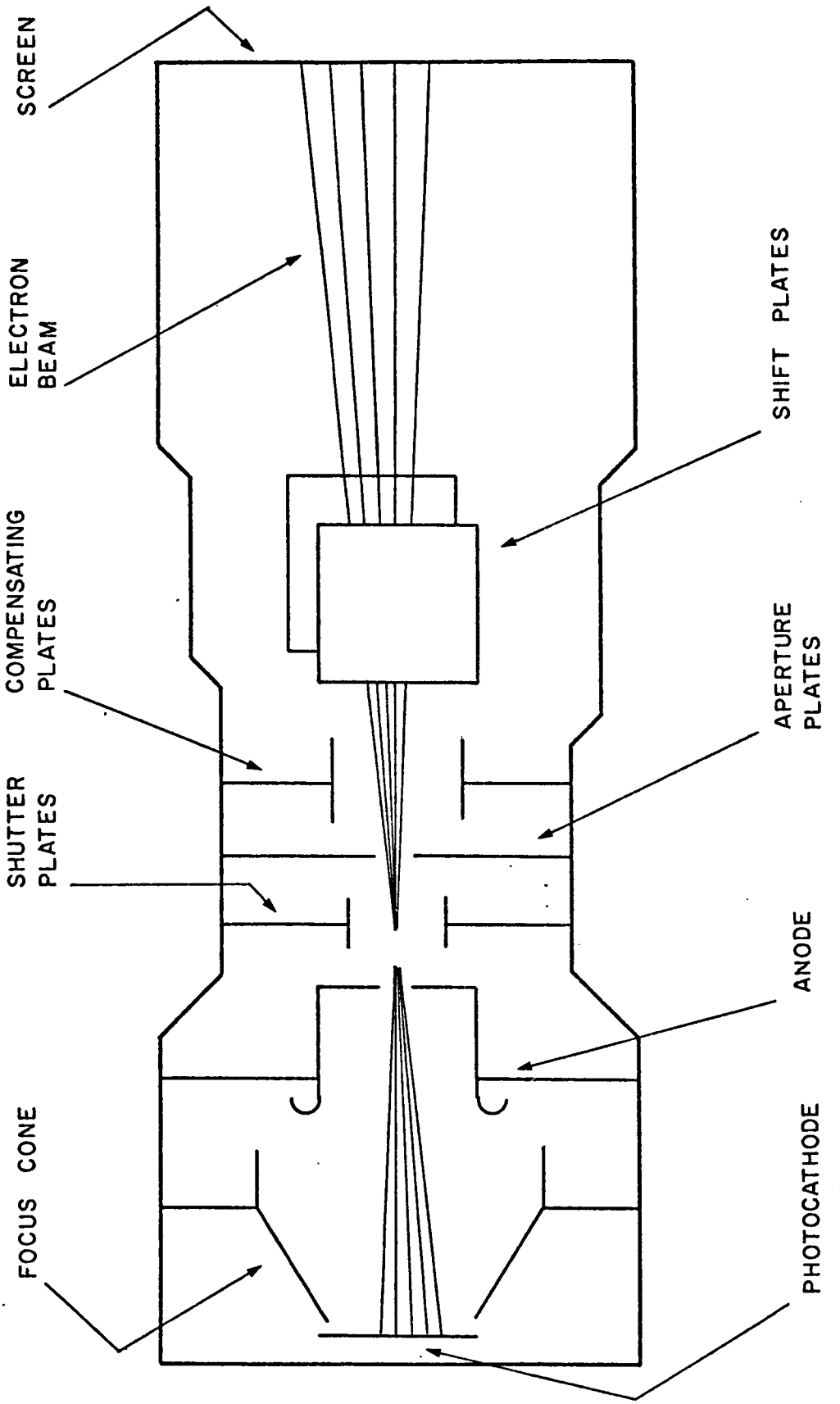
SCREEN
ELECTRON BEAM
SHIFT PLATES
COMPENSATING PLATES
APERTURE PLATES
SHUTTER PLATES
ANODE
FOCUS CONE
PHOTOCATHODE

beam off by deflecting it onto the aperture plates. A 201.25 MHz sinusoidal signal was applied to the compensating plates and shift plates so that the electron beam traced out a circular Lissajous pattern on the screen. This signal was produced by a local oscillator which was phase-locked to the accelerator RF signal. As a result, each circular sweep of the electron beam corresponded exactly to the 5nsec period of the accelerator beam.

The image converter tube screen was connected to the image intensifier by a high aperture coupling lens of 1:1 magnification. The image intensifier was a standard three-stage design which was magnetically focused to keep the noise level as low as possible. When operated at 35kv this unit had a gain of 10^5. A standard Polaroid roll-type film back with a Wollensak Oscillo Raptar 88m f/1.4 mounted in a Pi-Alphax shutter was used to photograph the third stage screen of the image intensifier. The complete system was mounted on a four foot long optical bench.

The expected number of photons reaching the film per photoelectron can be calculated from the Table I data with the aid of Figure 6.

$$\begin{aligned} \#\ \text{photons} &= G_1G_2\,E_1E_2 \\ &= 6 \times 10^2 \times 10^5 \times .02 \times .02 \qquad \text{(III-1)} \\ &= 2.4 \times 10^4. \end{aligned}$$

Figure 6: A schematic of the complete camera system. The numbers below show the intensity of photons at different sections of the system produced by a single photoelectron.

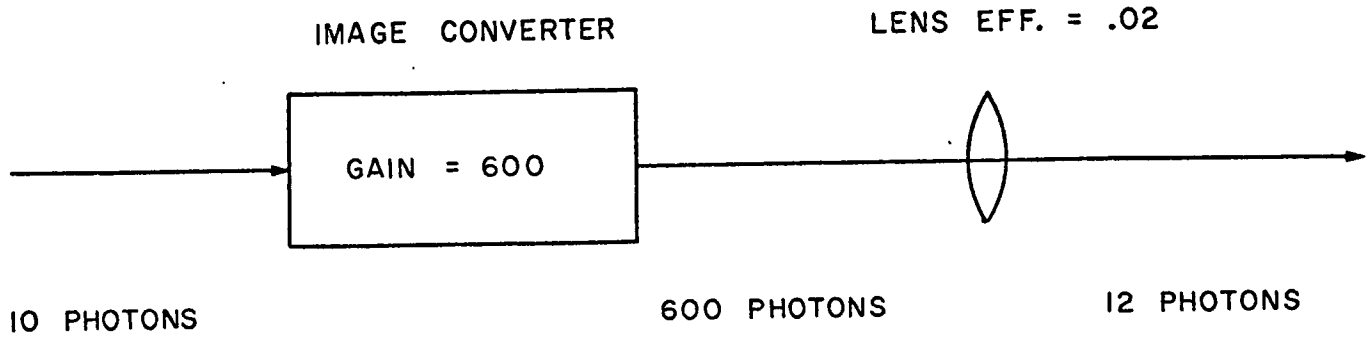
IMAGE CONVERTER
LENS EFF. = .02
GAIN = 600
10 PHOTONS
600 PHOTONS
12 PHOTONS

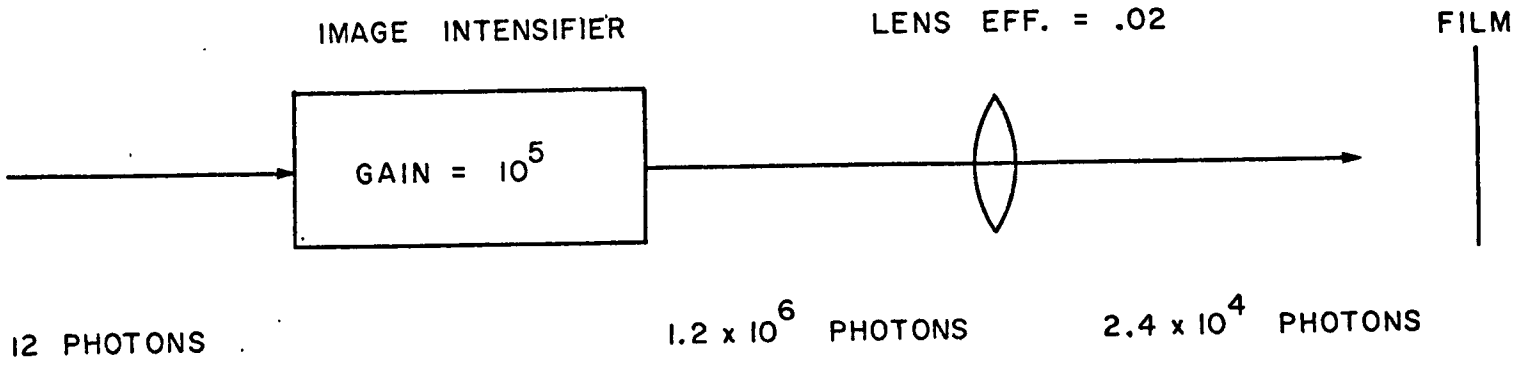
IMAGE INTENSIFIER
LENS EFF. = .02
FILM
GAIN = 10^5
12 PHOTONS
1.2×10^6 PHOTONS
2.4×10^4 PHOTONS

Here G1 and G2 are the gains of the tubes and E1 and E2 are the efficiencies of the lenses. In the wavelength region of interest the efficiency of the photocathode is about 1 photoelectron per 10 photons. The film used, Polaroid 410, requires 5×10^8 blue photons/cm^2 to produce a density change of 0.5. Since the 2.4×10^4 photons fall in a 100μ diameter spot, a single photoelectron records on film. Thus, the sensitivity of the complete system should be sufficient to detect any event which produces ten or more photons at the photocathode.

The dynamic range of the camera was not a critical factor because various gains could be adjusted and the exposure time for the film was variable. However, the signal to noise ratio (discussed below) was extremely critical. Both of the tubes in the camera were sources of noise. One of the major goals of the experiment described below was to evaluate the performance of the camera in terms of its signal to noise ratio and sensitivity.

B: Application of Theory

The intensity of the circular trace as a function of position along the circumference was the function $g(s,x_o)$ of equation II-35. The integration in this formula was performed by the recording film. Each sweep of the image

around the circle corresponded to one period of $f(t,x_o)$. Because the sweep rate was synchronized by a signal which was phase-locked with $f(t,x_o)$, the value of $g(s,x_o)$ for a particular s_o was given by

$$g(s_o,x_o) = \sum_m f(t_o + mT,x_o). \qquad \text{(III-2)}$$

The expected time resolution of the camera system depended on several factors:

1. Beam characteristics
2. Characteristics of the particle detector
3. Coupling between the detector and the camera
4. Camera characteristics
5. Data processing

The physical size of the beam flux and the size and shape of the particle detector affected the time resolution because the light produced by spatially separated, simultaneously occuring particles reached the camera at different times. This effect was estimated to be about .25nsec for the set up described in sections C and D. Another beam characteristic which affected the time resolution was the duty factor for the microperiod; i.e., even if the flux contained particles of only one velocity they would occupy approximately .25nsec of the 5nsec period (section C). As a result of these two effects it was expected that about

10% of the circular trace would receive light due to the main velocity component of the beam (the pions).

Thus, the time resolution of the system depended on the precision with which the angular position of the 10% exposed section of the trace could be determined. The angular resolution for a point source can be estimated from the manufacturer's data. For a circular trace diameter of 40mm about 400 points can be resolved around the circumference. Thus, the angular resolution was better than a degree. The coupling between the particle detector and the camera also affected the time resolution because the size of the image depended on this coupling. This point will be further discussed in section F. According to the manufacturer, the time jitter of the complete system was approximately 4.5psec. This small a time jitter did not appreciably affect the results. The data processing (Point 5 above) will also be discussed in section F.

There were two sources of noise in the system: the image converter tube photocathode and the intensifier tube photocathodes. Neither one of these sources had a periodic structure and hence the analysis of section II-C may be applied to show that the signal to noise ratio was improved for every period recorded. The improvement, however, was limited by the dynamic range of the film. For example, in

the case of a large noise amplitude relative to the signal amplitude, the average noise level, $L\bar{N}$ (see section II-C), would have overexposed the film before L could have become large enough to significantly improve the signal to noise ratio. This situation was experimentally encountered (section E) and required adjustments within the equipment to reduce the noise level.

C: Description of the Accelerator Beam

The particle flux for this experiment was provided by the Test Channel beam located in experimental area A at LAMPF.[5] This secondary beam, produced by the main beam at target A1, contained pions, muons, electrons, and protons. It had the same fundamental frequency and time structure as the main beam (Figure 2). The momentum, focus, and intensity of the particle flux in the channel's target area were controlled by a bending magnet, two quadrapole magnets, and a set of beam slits, respectively (Figure 7). The momentum range available was 100 Mev/c to 550 Mev/c with a resolution of approximately 2%.[19] The bending magnet polarity was reversible to allow the choice of a negatively or positively charged beam.

For the Imacon camera experiment the beam momentum was set at 350 Mev/c and a positive polarity was chosen because

Figure 7: Experimental Area A at LAMPF. The Test Channel used for the Imacon camera experiment is located in the lower center portion of the figure. The approximate location of the camera stand is shown by a rectangle marked by a C. Note the positions of the bending magnet, BM1, and the quadrapole magnets, Q1 and Q2.

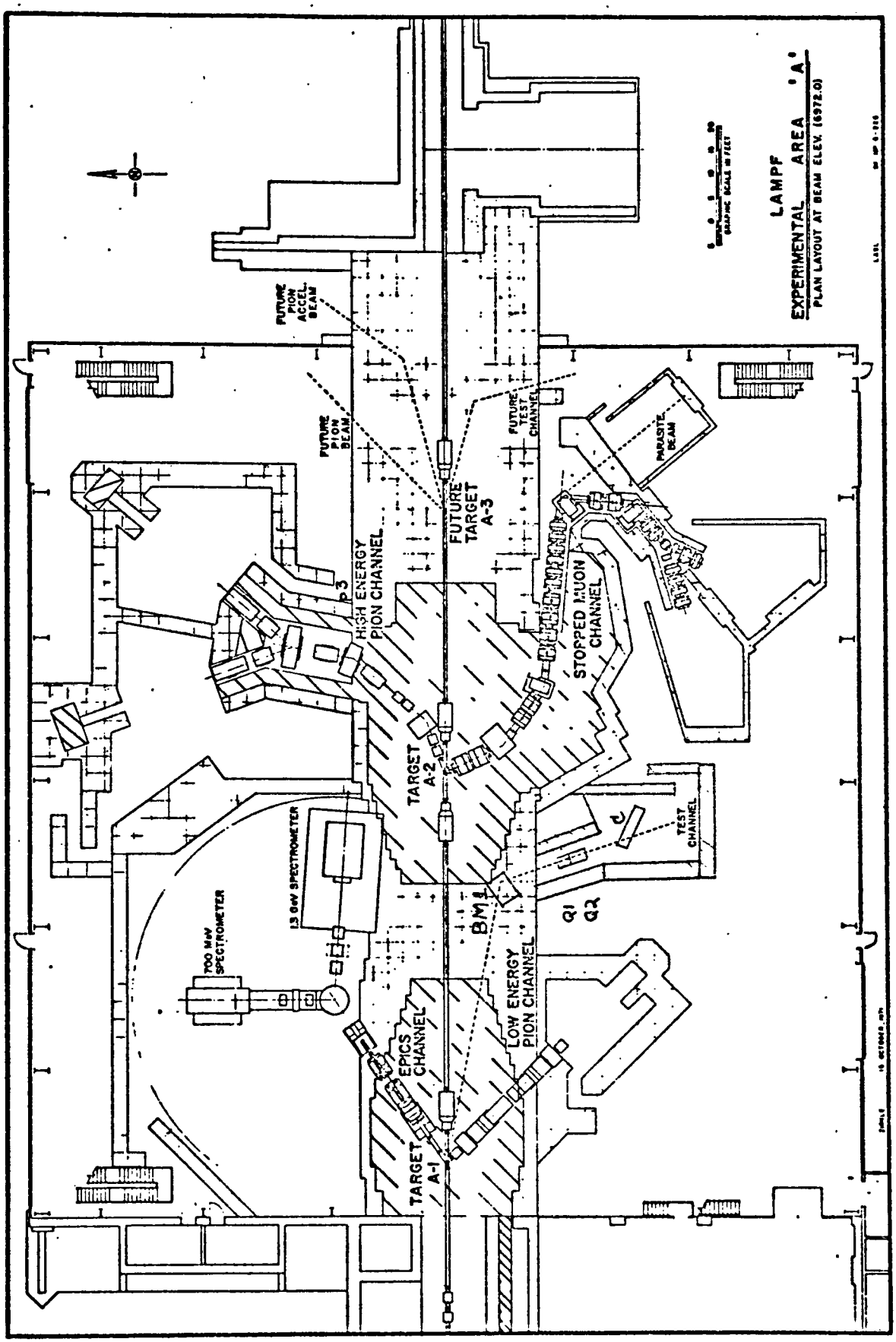
LAMPF
EXPERIMENTAL AREA 'A'
PLAN LAYOUT AT BEAM ELEV. (6972.0)
FUTURE PION ACCEL. BEAM
FUTURE PION BEAM
FUTURE TEST CHANNEL
PARASITE BEAM
HIGH ENERGY PION CHANNEL
P3
FUTURE TARGET A-3
STOPPED MUON CHANNEL
TARGET A-2
TEST CHANNEL
13 GeV SPECTROMETER
700 MeV SPECTROMETER
BM1
Q1
Q2
EPICS CHANNEL
LOW ENERGY PION CHANNEL
TARGET A-1

these settings provided the maximum pion flux.[19] Table II lists the particle fluxes expected at 350 Mev/c for a main beam current of 10μa. After a convenient position for inserting the camera into the beam was chosen, the two quadrapoles were adjusted to give the maximum focus at this spot. This was done by placing a thin 4" x 4" scintillator in the beam and optimizing the counting rate by adjusting the quadrapole currents. After the highest count rate was obtained a piece of Polaroid film was exposed to the beam for 10 minutes. The developed film showed that the beam spot was roughly 2.5" in diameter. Finally, the area around the beam line was roped off to prevent personnel in the target room from inadvertently wandering into the beam. The radiation level in the working area was checked by Health Physics and found to be at a safe level.

The accelerator RF synchronizing signal was provided through a 50Ω cable with an amplitude of 10 volts. This signal was phase-locked to the beam; i.e., any slow phase variations were present in both the beam phase and signal phase simultaneously.

D: Choice and Design of Light Producer

Two important factors considered in choosing the type of light producer for this experiment were 1.) the number

Table II: Particle fluxes for the Test Beam channel with beam jaws open to maximum position and quadropole focusing. Also shown are particle velocities and Čerenkov angles. Beam momentum for these measurements was 350 Mev/c for a main current of 10μA. The angle θ was calculated for n = 1.50.

Particle	Approximate Intensity	β	θ
π^+	5×10^5/sec	.929	44.14°
μ^+	5-10% of π^+ flux	.958	45.90°
e	$\ll \pi^+$ flux	1.00	48.19°
P	1.5×10^6/sec	.350	none

of photons produced per particle, and 2.) the time duration of the light output per particle. According to the manufacturer's data in Table I a single particle must produce a minimum of 10 photons at the photocathode in order to record on film. A fast organic scintillator, such as NE 111, is easily capable of producing this intensity per particle. However, as shown in Figure 8, even this extremely fast scintillator has a long tail which would have seriously affected the time resolution of the camera.[22] This is so because the camera would record the entire output of the scintillator. For this reason a Čerenkov radiator was chosen as the light producer best suited for this experiment. Since a Čerenkov radiator produces light only while a charged particle is actually traversing it, the time duration of the light pulse can be much less than 10^{-10} sec. The operation of Čerenkov radiators is discussed in Appendix C.

An acrylic UVT plastic with n = 1.50 was used for the Čerenkov radiator in this experient. From equation C1 the value of β_{min} was .67. Thus, for a beam momentum of 350 Mev/c only the protons did not produce Čerenkov light. The radiator was positioned at an angle θ with respect to the beam axis (Figure 9). The angle θ was calculated by using equation C2 for 350 Mev/c pions. The primary advantage of this geometry was that the light reaching the end

Figure 8: Pulse shape of the output of a fast scintillator, NE 111. The long tail makes this type of light producer unsuitable for use with the camera.

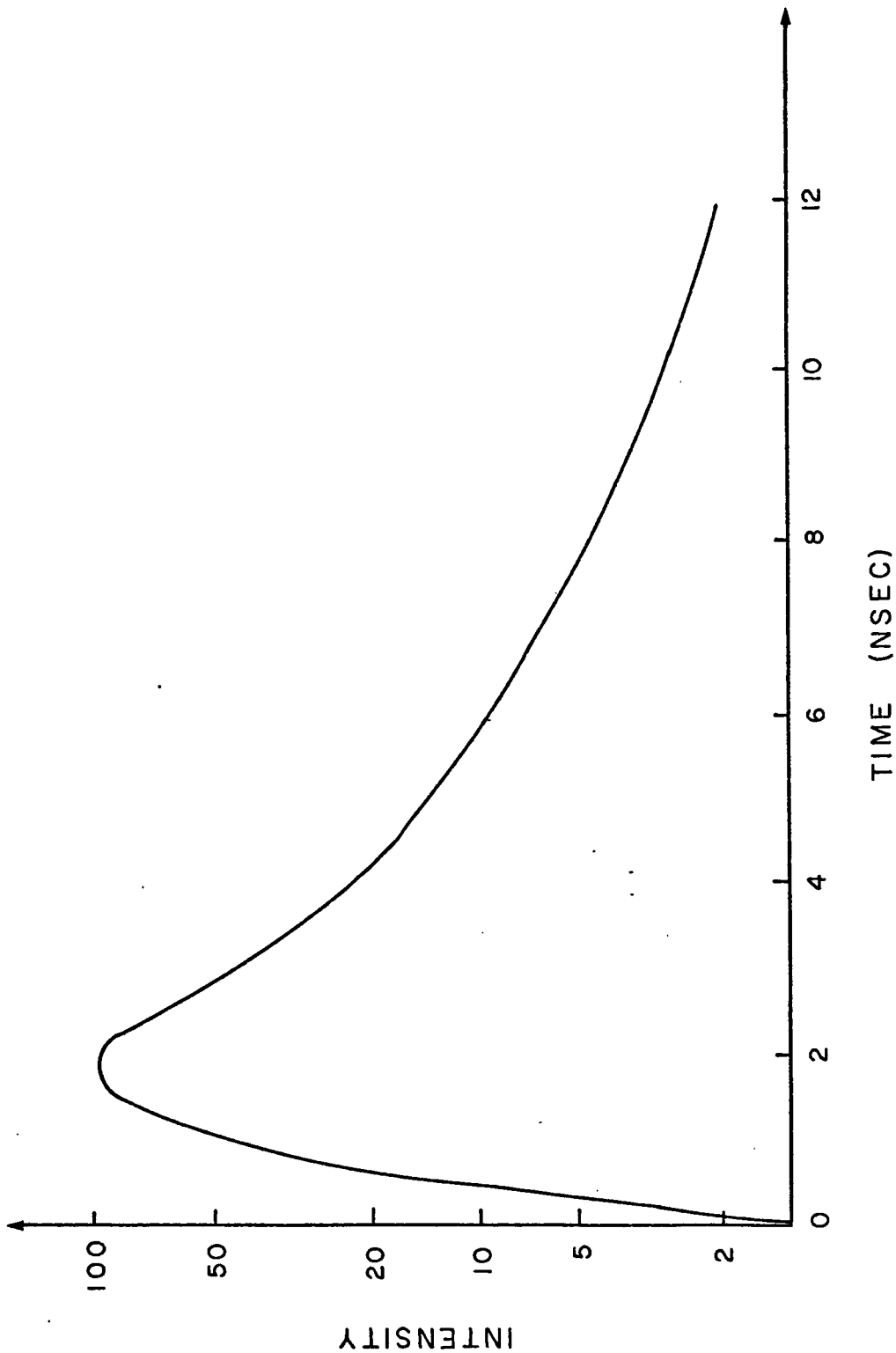
INTENSITY
100
50
20
10
5
2
0
2
4
6
8
10
12
TIME (NSEC)

Figure 9: The Čerenkov radiator. The radiator is angled with respect to the beam axis to produce maximum light transmission towards the camera.

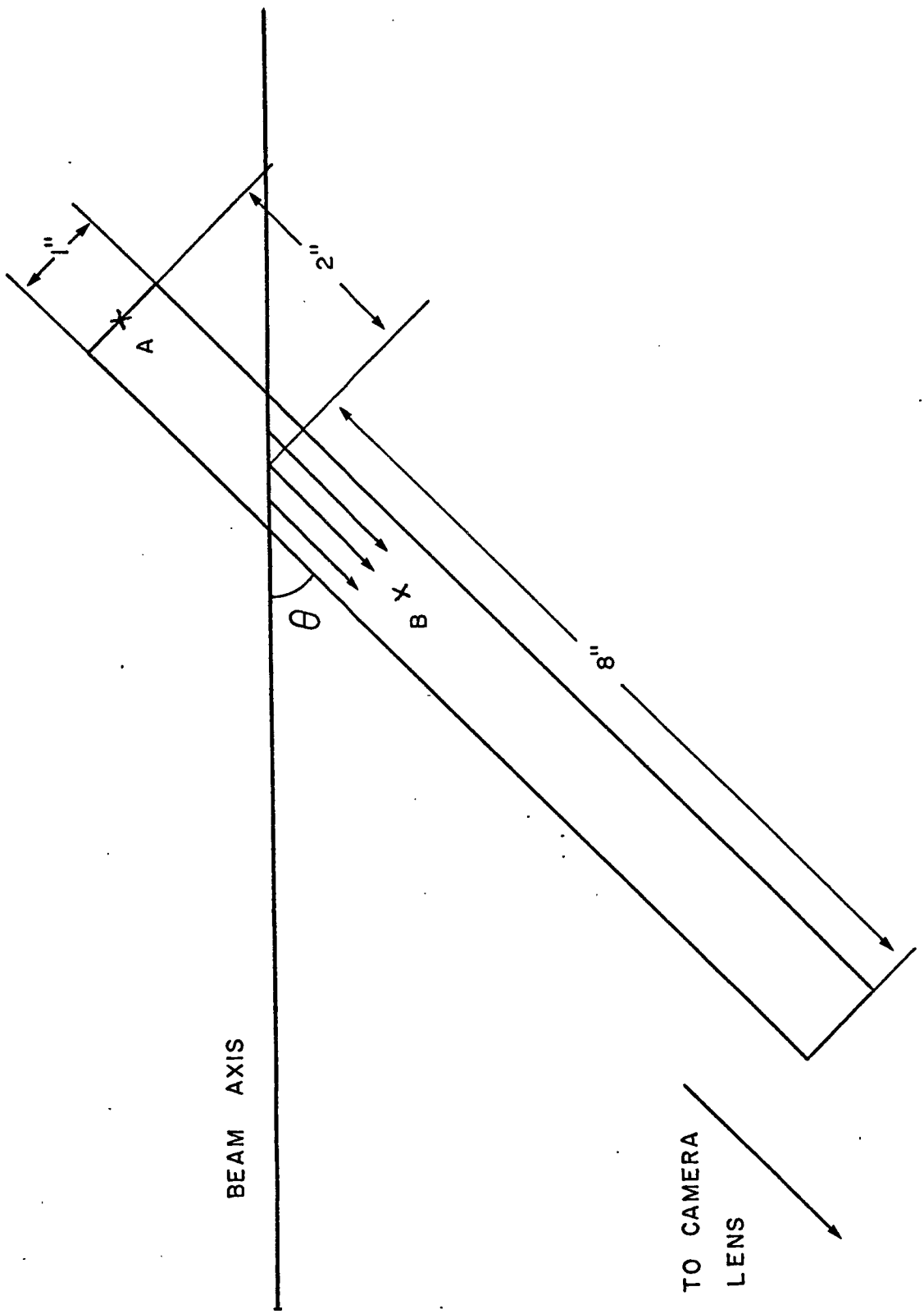
1"
2"
A
B
θ
8"
BEAM AXIS
TO CAMERA
LENS

of the radiator had the maximum possible transmission into air. Another advantage was a decrease in the time difference between pulses due to particles at opposite edges of the beam. This difference was calculated to be .25nsec for points A and B in Figure 9, whereas for the radiator fixed perpendicularly to the beam axis it would have been about .5nsec.

The number of photoelectrons theoretically produced per pion was calculated using equation C6. The lower wavelength limit was set at 3200 Å because beyond this range the transmission of the plastic rapidly approached zero. The upper wavelength limit, 5500 Å, was chosen because the photocathode efficiency falls off quite rapidly above this value. Furthermore, since only a lower estimate was needed, the efficiency $E(\lambda)$ was assumed to be a constant 10% through the wavelength range. The thickness of the material was $x = 3.66$ cm because of the slant with respect to the beam axis. The radiator had its first four inches of sides painted black to eliminate reflections from these surfaces. The other six inches were wrapped in aluminized Mylar. Thus, $G(\theta)$ was estimated by assuming that all photons entering the reflective section were reflected out the ends towards the camera lens. With the dimensions given $G(\theta)$ was approximately .120.

$N = (3.66/137)(.12)(.485)(.10)(.131 \times 10^5) \approx 2$ photoelectrons

The Čerenkov radiator was mounted in an aluminum light tight box (Figure 10) which was attached to the face of the camera chassis. The light emitting end of the radiator was 6" from the camera objective lens. This was the distance at which the lens used could collect all of the image onto the photocathode (see section E). The camera and Čerenkov holder were mounted on a movable cart at the beam height of 5 feet.

E: Procedure

The major objectives of the test runs of the Imacon camera done during a three day period at LAMPF were:

1. Verify proper phase synchronization of circular scan,
2. Measure the system's sensitivity to Č light,
3. Measure signal to noise level,
4. Evaluate overall performance.

This section describes the tests which were made, the problems encountered during the test runs, and their solutions.

After the camera system was assembled and initially checked out, the light tight box was bolted to the front face of the image converter tube chassis. A scintillator and light pipe assembly was attached to the box. This scin-

Figure 10: Top view of the camera system with Čerenkov radiator and light tight box attached.

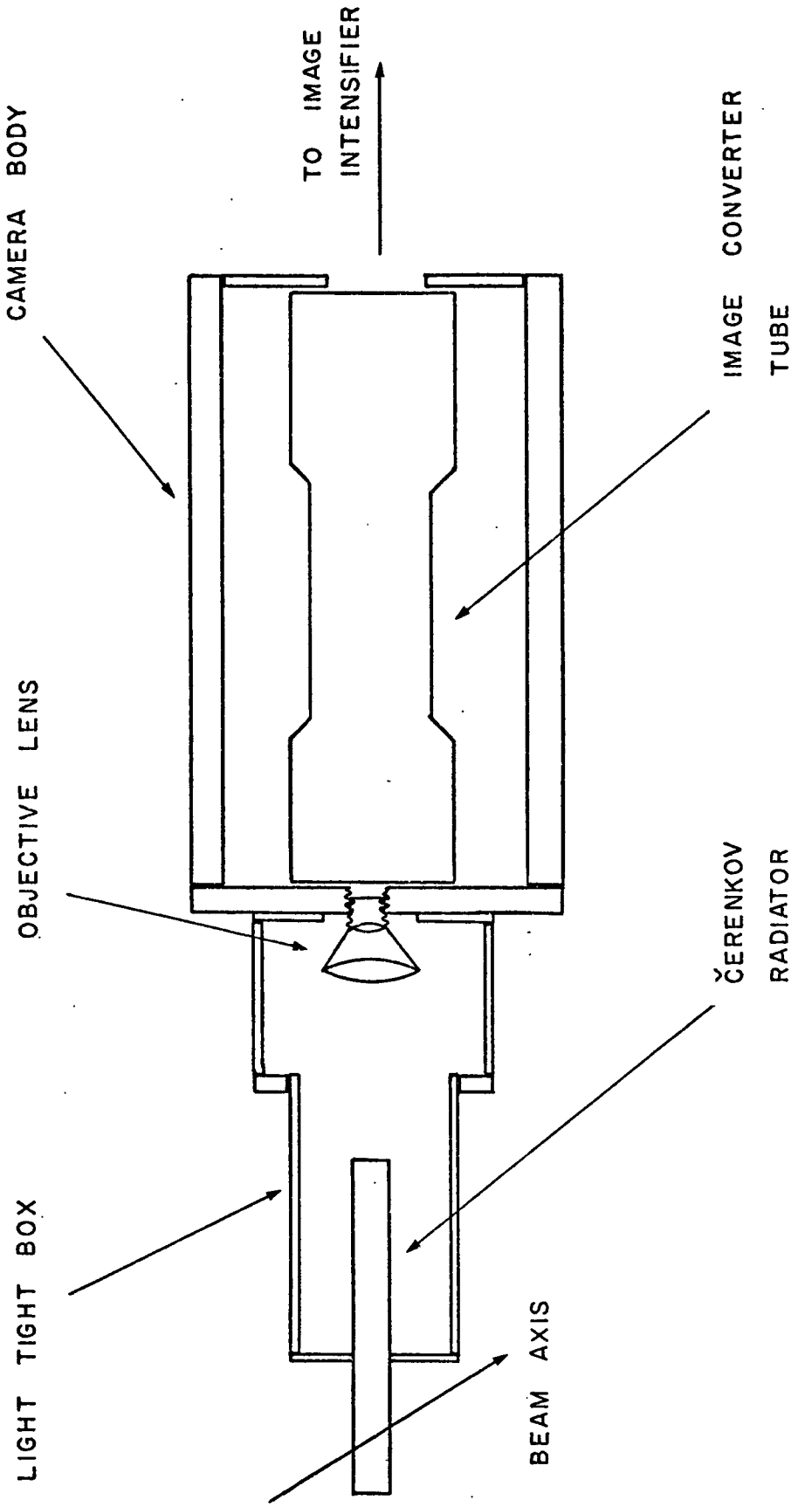
TO IMAGE INTENSIFIER
CAMERA BODY
IMAGE CONVERTER TUBE
OBJECTIVE LENS
ČERENKOV RADIATOR
LIGHT TIGHT BOX
BEAM AXIS

tillator was used with a Co^{60} source to provide a light source for testing the two objective lenses which were available. These were a 1.5mm focal length reflective microscope objective and a 18mm, wide aperture lens. As each lens was mounted to the camera, a light emitting diode was placed at the end of the light pipe to provide an intense enough source for focusing purposes. After taking several Polaroid photographs with each lens in place the conclusions reached were:

a.) The 18mm lens had better light collection and efficiency by a factor of three.

b.) The 1.5mm lens produced an image one-half the size of the 18mm lens image.

Since the response of the camera to the low intensity Č light was virtually unknown, it was decided to sacrifice the better focus in favor of larger larger light collection. During these tests it was observed that after exposure to high level light such as the LED or the room light the photocathode of the image converter tube retained an after image which would gradually fade after several hours.

Next, the test channel beam was set for a 350 Mev/c momentum and was focused by the procedure described in section C. The scintillator was removed from the box and the Čerenkov detector (Figure 9) was installed. With the circu-

lar scan not operating, several photographs were taken with the beam on and off and also as the angle of the detector with respect to the beam axis was varied. Since the image recorded changed as the angle varied it was verified that Č radiation and not any other effect was being seen. Figure 11 shows a 10 second exposure taken with the angle set exactly at the Č angle for pions.

With the beam off, the RF voltage which controlled the circular scan was turned on and adjusted. This caused a very high noise level in the image converter tube (Figure 12) which was intolerable for any useful results. The source of this noise was eventually traced to RF pickup between the deflection plate cables and the shutter plates' electronics. This problem was partially solved by rerouting and shortening the cables. However, in order to completely remove the noise the RF voltages had to be decreased in intensity. This resulted in a circular scan diameter of 10mm rather than 40mm.

After the RF pickup problem was solved, the circular scan and the beam were turned on and a set of four photographs were taken (Figure 13). The length of the sync cable was altered between these pictures so that there was a difference of 1nsec between them. The camera and detector were then repositioned 10" down the beam axis and an addi-

Figure 11: A 10 second exposure without the circular scan. This photograph represents the effect of the Čerenkov radiation due to a 350 Mev/c pion beam with an intensity of 4×10^5 pions/sec.

Figure 12: The RF pick-up noise which initially occurred when the circular scan voltages were applied to the image converter tube plates.

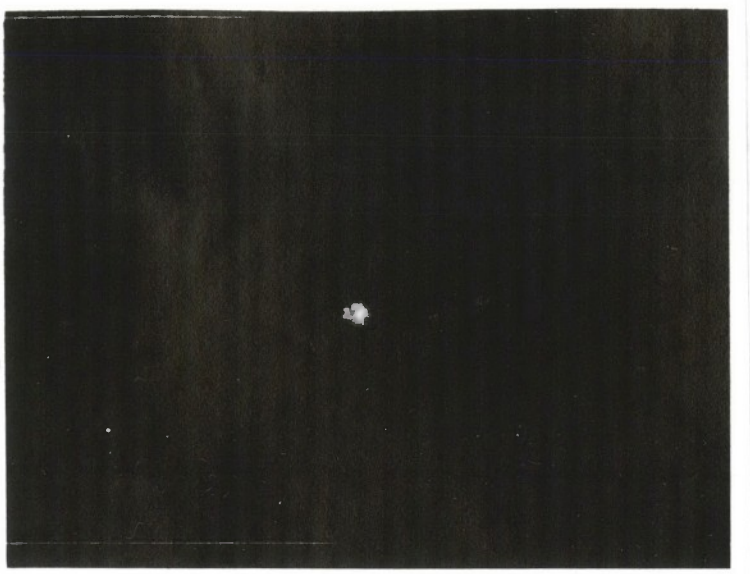

Figure 11

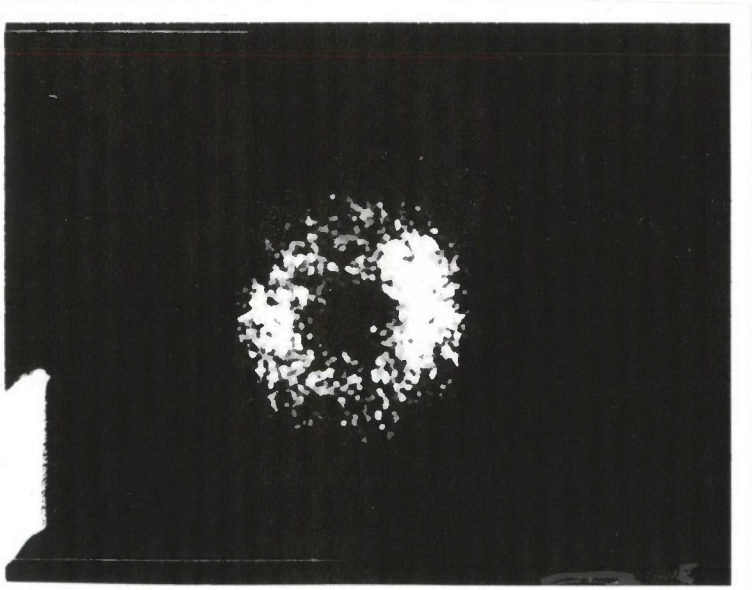

Figure 12

Figure 13: A series of photographs taken at different sync signal delays with circular scan (10 sec exposures).

A. No delay

B. 1 nsec delay

C. 2 nsec delay

D. 3 nsec delay

These delays are only approximate (see text) values.

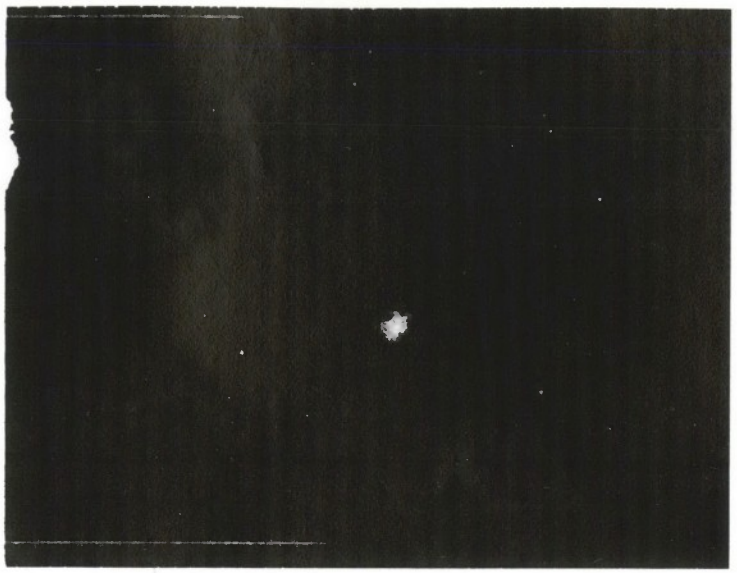

Figure 13a

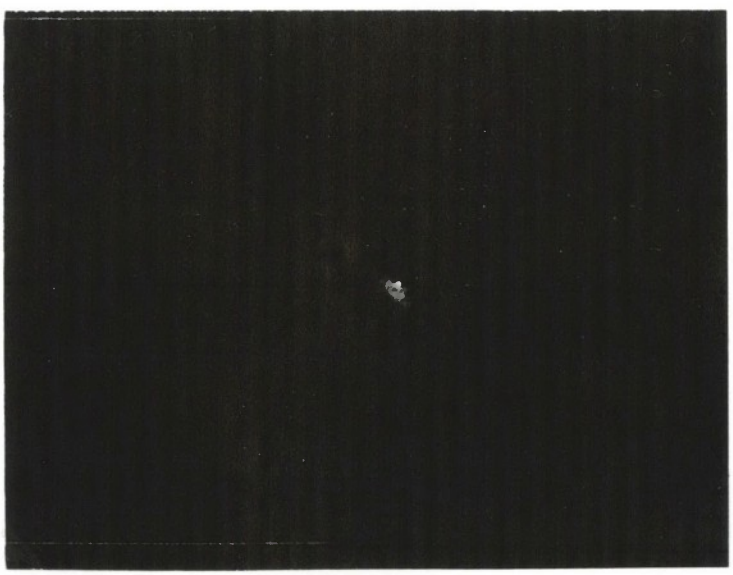

Figure 13b

Figure 13c

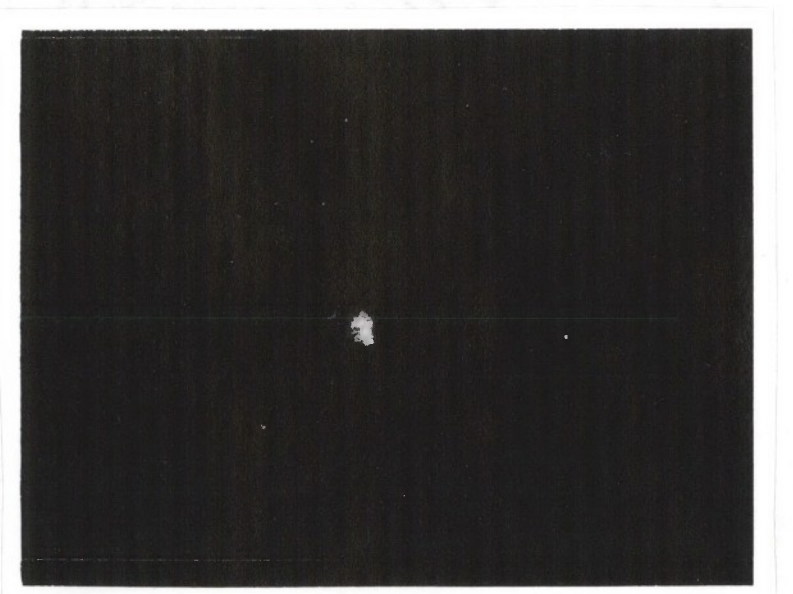

Figure 13d

tional set of four photographs was taken. One of these is shown in Figure 14 and should be compared to Figure 13B.

Many other photographs (not shown) were taken with varying exposure times, different angle settings, and at a different beam momentum.

Initially, it had been planned to take photographs with negative type film. However, because of a lack of beam time there was not sufficient time to refocus the system with a different film backing and allow the residual noise to decay away. Also, there was not sufficient time to use a scintillator to detect the protons in the beam.

F: Results and Discussion

After carefully examining the photographs shown in Figures 13 and 14 it was decided that no essential additional information could be obtained by examining them with a microdensitometer. The reasons for this decision were:

1. The size of the image effectively masked any detailed structure within the exposed areas.
2. The shape of the images changed as the phase of the synchronizing signal was varied.
3. The intensity of the image was not constant around the trace.

Points 2 and 3 indicate that the operation of the camera

Figure 14: This photograph was taken under conditions similar to Figure 13B except that the camera was repositioned 10 inches further along the beam axis.

Figure 14

system was not uniform around the circular pattern. This possibly could have been due to a remaining RF pickup problem since Figure 12 does show an intensity variation. The results discussed in this section are qualitative; however, they do allow some conclusions to be drawn.

Figure 11 can be used to estimate the sensitivity of the system. From Table I the approximate total pion flux in the beam was 5×10^5 pions/sec. Since the beam had a circular cross sectional area of 2.5" diameter, the Č detector intersected the path of only about 75% of the particles. Thus, the light in Figure 11, a 10 second exposure, represents the result of approximately 4×10^6 pions. Several photographs that were taken for lower beam intensities and longer exposure times indicate that the noise level became appreciable to the signal level for a flux of about 10^4 particles/sec. However, this figure is very dependent on the geometry of the set up. This is so because a decrease in the image size would result in more light per unit area and hence increase the signal to noise ratio. This is only true for the noise added from sources other than the image converter photocathode. With the present set up the sensitivity and total noise of the system limited its usefulness to flux rates above 10^4 particles/second.

In Figure 15 the outlines of the exposed areas of

Figure 15: The data of Figure 13 plotted on a scale enlarged by a factor of five. The letters on the figure correspond to the parts of Figure 13.

Figure 16: The data from Figure 13B and Figure 14. This plot was used to estimate the pion velocity.

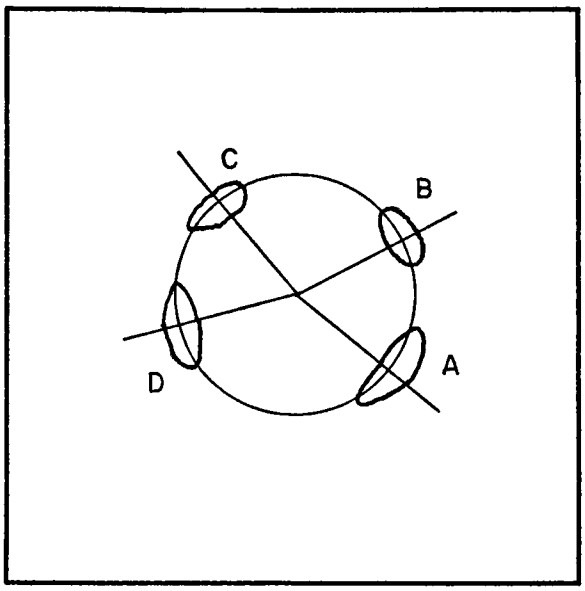

FIGURE 15

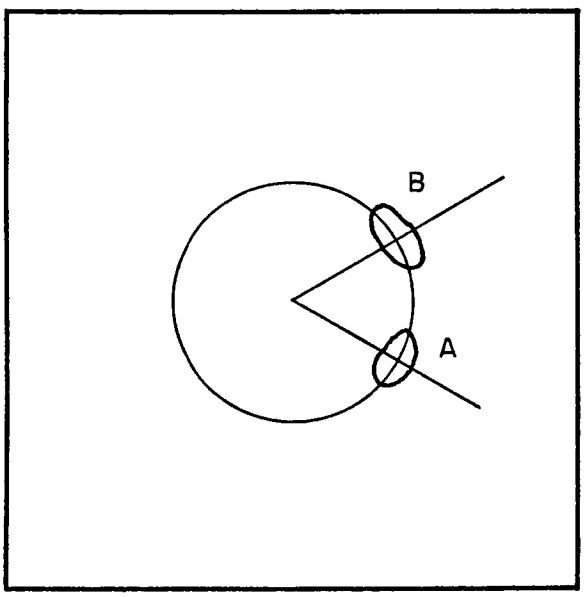

FIGURE 16

Figure 13 are combined on a scale enlarged by a factor of five. The sync signal delay was 1nsec between adjacent areas. The facts that for each of the photographs only a small portion of the circular trace received light and that the position of the exposed area changed when the phase of the sync signal was altered indicates that the circular trace was, indeed, phase-locked to the sync signal. Figure 16 is a combination of Figures 14 and 13B and can be used to estimate the velocity of the particles that were detected.

$$\beta = d/\Delta tc \approx .95$$

Here d = 10", the distance along the beam axis between the two placements of the camera, and $\Delta t \approx .9$nsec from the figure. This value of β agrees somewhat with the β for 350 Mev/c pions. The velocity of the particles can not be measured from the data taken at a single camera position because there was no way of establishing a reference phase angle between the beam flux and the sync signal.

In Figure 17 the angular position of the center line of each exposed area in Figure 15 has been plotted versus the time delay. A least squares straight line fit to these points gives a slope of 78.1°/nsec which should be compared to the theoretical value of 72°/nsec. Because of the changing shapes and sizes of the exposed areas it has been esti-

Figure 17: A plot of the angular positions of the data in Figure 15 versus the time delay. The solid line is the result of a least squares fit. The dashed line is the theoretically correct value.

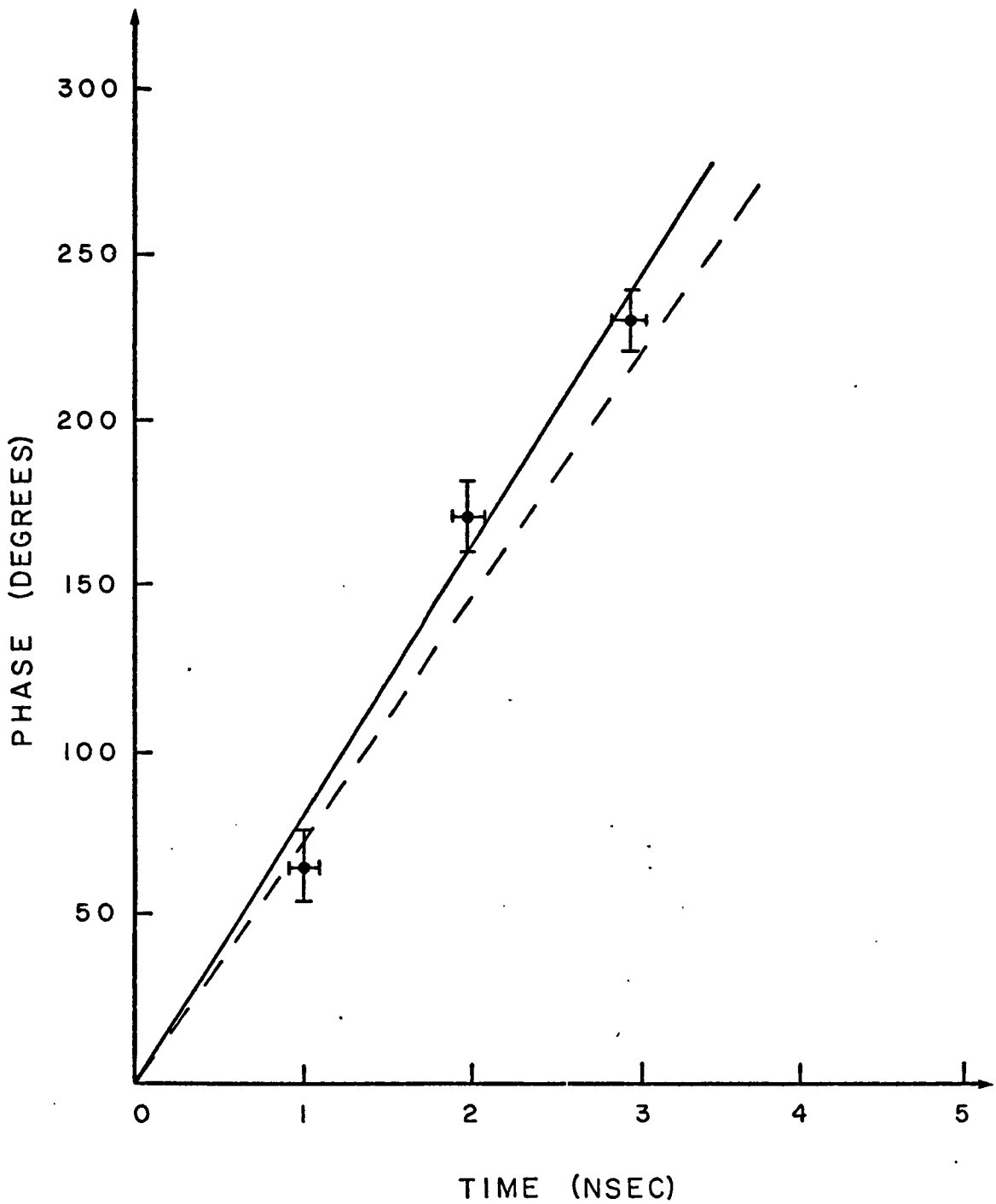
300
250
200
150
100
50
PHASE (DEGREES)
0
1
2
3
4
5
TIME (NSEC)

mated that the angular position cannot be determined better than ± 10°. Also, there is an uncertainty in the time delay which can be traced to slight variations in the cable lengths and the effects of the connectors used to attach the delay cables.

The muons in the beam also produced Čerenkov light. With the geometry used, the angular difference of 1.8° between the pion and muon Č radiation was not enough to affect the detection of the muon light. However, since the pions decayed randomly in time the muons did not have a very definite time structure. In fact, for the beam used, a simple calculation shows that the muon distribution was evenly spread out over about 180° of the circular trace preceeding the pions. The results of the photographs in this region of the trace are too nebulous to make any definite conclusions about whether the muons can be seen by the system.

The following conclusions can be drawn from the analysis of the results of the Imacon camera experiment:

1. The camera system does have sufficient sensitivity and signal to noise ratio to be useful for detecting Č light.
2. The phase-locking by the sync signal worked correctly.
3. The system had some severe problems which would

need to be corrected before any really useful results could be obtained. The most obvious of these is the non-uniformity in the images displayed in Figure 15. The only physical difference between the data points in this figure was a change in the length of the sync signal cable. A possible source of this non-uniformity was an unequal magnitude between the X and Y sync signal components. The result would be a distorted circle and could account for the apparent symmetry of the images in Figure 15. Other minor problems were insufficient RF shielding, no external means of focusing, and light leaks.

4. In order to ever become capable of giving quantitative results the detector and objective lens geometry would have to be redesigned to provide a much smaller and better focused image.
5. Even if the above improvements are made and a detailed time structure can be detected there would still be serious problems interpreting the data. This is so first of all because for β's in the range of .75 or more, the relative phases of different velocity components changes very little with any reasonable distance along the flux axis.

Secondly, the physical extent of the beam tends to mask the time structure unless some geometry can be found to over come this effect. Thirdly, the pulse width of the flux (.25nsec) tends to mask the time structure also. These last two effects could possibly be corrected by a proper data analysis.

In conclusion then, it is not very clear that this system could offer any definite improvements over standard particle-by-particle TOF time resolution for anything but simple velocity distributions. Its one advantage is that problems due to pile-up can never occur. Hence, it seems likely that the camera could best be used in an application such as a beam monitor.

In the following chapter a method of velocity component phase detection is proposed. This system seems to be capable of avoiding many of the problems associated with the Imacon camera.

IV: RF PHASE DETECTION

This chapter consists of a proposal for a method of finding TOF spectra of time coherent particle fluxes which uses correlation detection and RF techniques to measure the phases and amplitudes of the velocity components in the flux. Section A describes the operation of an electronics system which is used to process the measured flux signal. The frequency at which the system operates is that of the LAMPF accelerator. In section B the theory of section II-C is applied to a discussion of the system and its merits. Finally, a possible detector design is presented in section C.

A: Electronics System

It will initially be assumed that the periodic particle current is measured and is given by the noise-free signal $f(x_o,t)$ of equation II-33, and that an accelerator oscillator signal $\cos\omega_o t$ is available. A schematic of a system which combines these two signals to produce the function $g(x_o,\tau)$ of equation II-40 is shown in Figure 18. There are three basic sections to this system. The function of block A is to transfer the amplitude and relative phase information of $f(x_o,t)$ to a lower frequency ω_s, which is supplied by a local oscillator. The intermediate signal generated

Figure 18: Block diagram of a system which uses RF techniques to measure the phase of a time coherent particle flux.

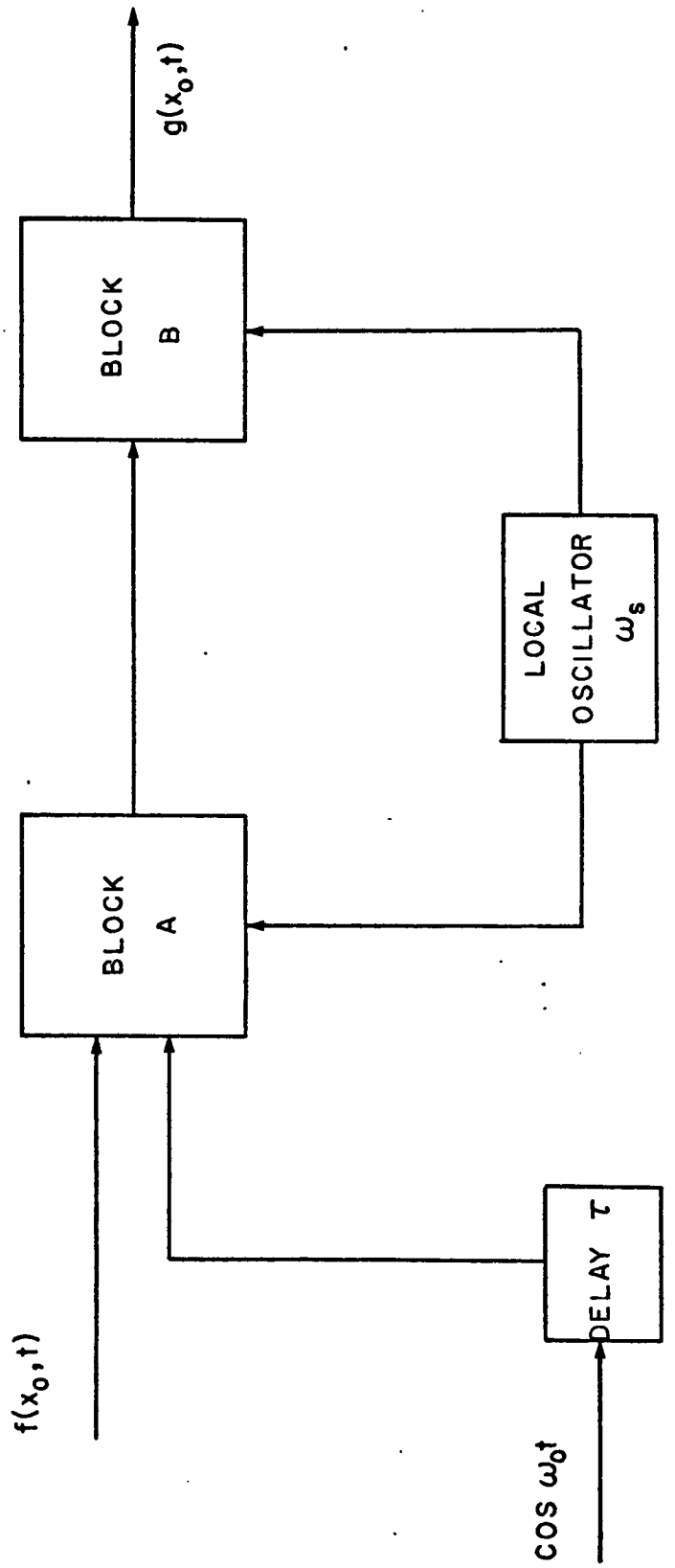
$g(x_0,t)$
BLOCK B
LOCAL OSCILLATOR ω_s
BLOCK A
$f(x_0,t)$
DELAY τ
COS $\omega_0 t$

in block A is recombined with the local oscillator signal in block B which produces $g(x_o,\tau)$.

The advantages of introducing an intermediate frequency, ω_s, are the same as those found in the design of radio receivers; i.e., improved selectivity and higher gain in the amplifiers.[23] The maximum stable gain of an amplifier is greater at lower frequencies because capacitative feedback is less. The selectivity of a tuned circuit is a measure of its bandwidth, which is given by

$$B = f_r/Q \qquad \text{(IV-1)}$$

where f_r is the resonant frequency. For a given Q value the selectivity increases as f_r decreases. Another major advantage of the design in Figure 18 is that (as will be seen below) phase and frequency fluctuations in the local oscillator do not affect the final output.

The individual components of block A are shown in Figure 19. The operation of this circuit is easily described by assuming that $f(x_o,t)$ contains only a single velocity component. The RF amplifier is narrowly tuned about ω_o and has a gain of about 50. Its output, therefore, is proportional to $A\cos(\omega_o t + \varphi)$ where A and φ are the amplitude and phase of the velocity component of $f(x_o,t)$. (For simplicity, in this discussion all proportionality constants and additive constants are set equal to one and zero, respectively).

Figure 19: The components in block A of Figure 18. The phase and amplitude information contained in $f(x_o,t)$ is transferred to a lower frequency, ω_s.

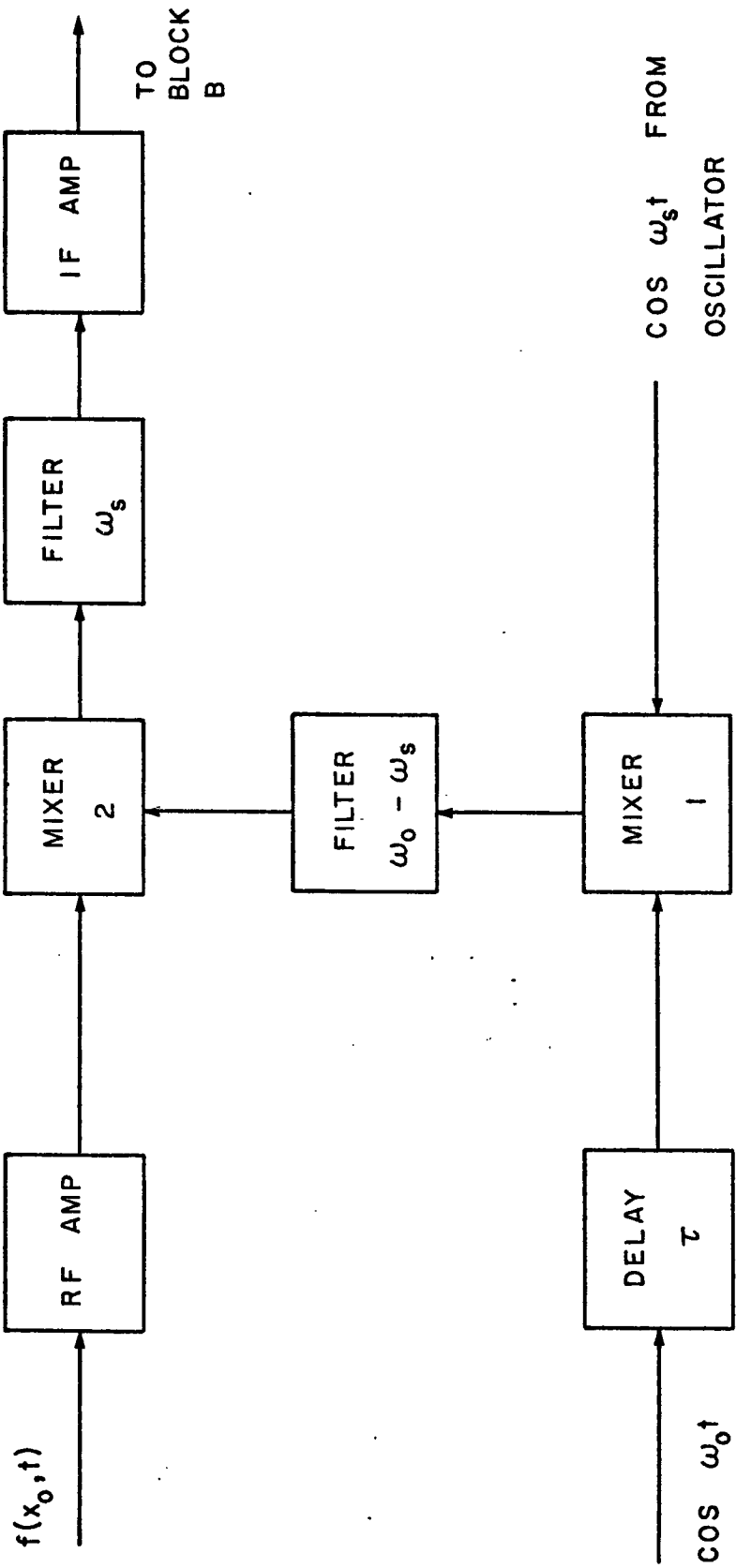
$f(x_o,t)$
RF AMP
MIXER 2
FILTER ω_s
IF AMP
TO BLOCK B
COS $\omega_o t$
DELAY τ
MIXER 1
FILTER $\omega_o - \omega_s$
COS $\omega_s t$ FROM OSCILLATOR

The purpose of the narrow bandwidth of this amplifier is to filter out the harmonics of ω_o and reduce the spectral extent of the noise component input to mixer 2.[23]

The mixers are both square-law mixers which means that for any two inputs f_1 and f_2, the output is given by $f_1 + f_2 + (f_1 + f_2)^2$. The output of mixer 1 is

$$m_1(t) = \cos(\omega_o t + \theta) + \cos\omega_s t + \cos^2\omega_s t + \cos^2(\omega_o t + \theta) + 2\cos\omega_s t\cos(\omega_o t + \theta). \quad \text{(IV-2)}$$

Here, the phase angle θ is equal to $\omega_o\tau$ and is externally adjustable. When $m_1(t)$ is filtered at the frequency $\omega_o-\omega_s$, the result is $\cos((\omega_o-\omega_s)t + \theta)$.

This signal is combined with the measured flux current signal in mixer 2 to produce

$$m_2(t) = A\cos(\omega_o t + \varphi) + \cos((\omega_o-\omega_s)t + \theta) + A^2\cos^2(\omega_o t + \varphi) + \cos^2((\omega_o-\omega_s)t + \theta) + 2A\cos((\omega_o-\omega_s)t + \theta)\cos(\omega_o t + \varphi). \quad \text{(IV-3)}$$

If this output is filtered at the frequency ω_s, the only component passed is

$$A\cos(\omega_s t + (\varphi-\theta)). \quad \text{(IV-4)}$$

Thus the amplitude and phase of $f(x_o,t)$ have been transferred to a lower frequency. The IF amplifier is sharply tuned

at ω_s with a gain of about 10^5.

Block B is a simple phase detector which produces an output proportional to the amplitudes of the inputs and the cosine of their phase difference. Thus, the output of the circuit in Figure 18 will be proportional to $A\cos\omega_o(\tau+x/v)$. By varying τ, the amplitude and phase can be found. By defining the phase of the output as the zero cross-over point, a very precise measurement can be made because the cosine function has its maximum slope at this point.

The local oscillator used to produce $\cos\omega_s t$ does not have to be extremely stable. This is so because any phase variations or frequency variations will be present at both inputs of the phase detector and will cancel out. To ensure that the variations have a minimum effect, the oscillator signal to the phase detector can be delayed so that it and the signal passing through the filters and mixers arrive at block B simultaneously.

If $f(x_o,t)$ contains more than one velocity component the analysis methods described in Appendix B can be used to extract the TOF spectrum from $g(x,\tau)$. This will require the detection system to be movable along the beam axis. By choosing ω_s = 10.7 MHz, the IF frequency of FM radios, most of the circuitry of Figure 19 can be taken directly from radio designs.

The following section considers some aspects of the operation of the system in more detail.

B: Application of Theory

It was pointed out in Chapter II that the function $f(x_o,t)$ represents the actual particle flux only in a statistical sense. Thus, it is important to analyze the system described above by considering its response to single particles. In all the previous chapters the results obtained by considering the input as either $f(x_o,t)$ or a sum of single particles contributions were identical. This is not necessarily true, however, for the system described in section A because the mixers are non-linear divices. In this section the particle detector and the RF amplifier are considered as a single unit described by its bandwidth and Q value.

If the detection device had an infinite Q value then the output due to a single particle would be an infinitely long sinusoidal wave. In reality, though, the system, when excited, produces a decaying sinusoidal. This means that in the frequency domain the signal is not a pure sinusoidal but has additional frequency components. When this signal is operated on by mixer 2 cross terms arise between the different frequency terms. Most of these terms are negligible

because their frequencies will be harmonics of ω_o. However, it is easily shown that here are also lower frequency terms whose frequencies vary from DC up to $\Delta\omega$ where $\Delta\omega$ is the bandwidth of the signal. In order for these terms to have a negligible effect on the whole circuit $\Delta\omega << \omega_s$. For example, if $\omega_s \approx$ 10MHz and ω_o = 200MHz then an acceptable value for $\Delta\omega$ is $\Delta\omega \approx$ 2MHz. Or using equation IV-1, the Q value of the detection circuit must be

$$Q = 200\text{MHz}/2\text{MHz} = 100 \qquad \text{(IV-5)}$$

This demonstration illustrates that the Q value of the system should be as high as possible.

One of the problems with the system described in Chapter III was that the phase distribution of each velocity component was folded into the measured time structure. It is instructive to discover how the phase distribution of a single velocity component will affect the operation of the circuit in Figure 19. Consider a chain of N particles producing an input to the phase detector of $\sum_N \cos(\omega_s t+(\varphi_N-\theta))$. The particles may or may not arrive at the detector at such a rate that their cosine waves overlap. In either case, the fluctuating phases will cause the output of the phase detector to vary. For this reason a simple phase detector will not suffice for measuring the average phase of the flux. Of course, this problem is not encountered with very intense

fluxes because in these cases $f(x_o,t)$ actually does represent the flux.

The problem can be circumvented by substituting a multiplier and an integrator for the phase detector. That is, the output of the circuit is given by

$$g(x_o,\tau) = (1/mT)\sum_N \int_o^{mT} \cos\omega_s t \cos(\omega_s t + (\varphi_N - \theta))dt, \qquad \text{(IV-6)}$$

or

$$g(x_o,\tau) = A \sum_N \cos(\varphi_N - \omega_o \tau) \qquad \text{(IV-7)}$$

$$= A \sum_N \cos(\omega_o x_o/v - \omega_o \tau + \Delta\varphi_N)$$

$$= A\cos\omega_o(x_o/v - \tau) \sum_N \cos\Delta\varphi_N \qquad \text{(IV-8)}$$

if the distribution of phases is symmetric. Thus, the phase of $g(x_o,\tau)$ is actually the average phase of the velocity component of the flux.

There are two sources of noise which can seriously affect the result of the measurement of a particle flux current made by the system described above. The first of these, external noise, is the noise which is present in the input signal to the RF amplifier. The internal noise, the second source, is the noise which is added to the signal by each circuit in the system. The magnitude of these two noise sources is difficult to predict in general. This is so be-

cause the external noise depends on the type of particle detector being used and its environment, and the internal noise depends on the circuit designs and their individual components. For these reasons, the discussion below is mostly qualitative and merely indicates the important aspects of the system design which will lead to the most favorable signal to noise ratio.

A convenient measure of merit for the sensitivity of a system is the noise factor, F, defined by the equation:

$$F = (S_i/N_i)^2/(S_o/N_o)^2 = S_i^2N_o^2/S_o^2N_i^2, \qquad \text{(IV-9)}$$

where S_1 is the input noise voltage, S_o, is the output signal voltage, N_i is the input noise voltage, and N_o is the output noise voltage. An ideal system would add no noise and would have an F equal to unity. The following argument shows that in a complex system consisting of several stages the major contribution to the noise factor comes from the first stage.

Consider a noise free signal, S, as the input to a two stage system with gains G_1 and G_2 and internal noise sources N_1 and N_2. The total signal output will be G_1G_2S and the total noise output will be $((G_1G_2N_1)^2 + (G_2N_2)^2)^{\frac{1}{2}}$. Thus, the output signal to noise ratio will be

$$S_o/N_o = G_1S/(G_1^2N_.^2 + N_2^2)^{\frac{1}{2}}. \qquad \text{(IV-10)}$$

If G_1 is large compared to unity and N_1 and N_2 have equal orders of magnitude, then

$$S_o/N_o \approx S/N_1. \qquad \text{(IV-11)}$$

Since these conditions do apply in the RF system described above, the noise factor of the system can be approximately estimated by considering only the noise contributed by the RF amplifier. Commercial receivers, using transistors or FET's in the RF amplifier, are capable of achieving a noise factor of $F \approx 2$.

There are two sources of external noise: thermal agitation in the particle detector and interference noise. The thermal noise, or Johnson noise, is a white noise which is due to the movement of the free charges in a conductor. The thermal noise in the particle detector is given by:

$$N_{rms} = (4KTRB)^{\frac{1}{2}}, \qquad \text{(IV-12)}$$

where K is Boltzman's constant, T is the temperature in degrees Kelvin, B is the effective bandpass of the noise, and R is the resistance across the detector.

Interference noise is picked up from the environment of the particle detector. Examples are: impulse noise, i.e., static caused by lightening, switching transients generated by electrical machinery, and radio frequency interference, i.e., interference due to broadcast radio-frequency

carriers or pickup of the accelerator RF frequency. Proper shielding of the detection apparatus should greatly reduce the effects of interference. The overall effect of impulse noise in the system depends on its bandwidth. If a narrow bandwidth system is used then only a small portion of the energy in an impulse can filter through.

The discussions of this section indicate that the optimum performance can be obtained by designing the system with as small a bandwidth as possible. FM radio receivers typically have a bandwidth of 240 KHz. This bandwidth allows the detection of all the sideband information that is generated by the modulation of the carrier signal. For the particle detection system, however, this extra bandwidth is not required and, hence, the system should be capable of achieving extremely low noise levels.

C: The Detector

From the preceeding section it is evident that the maximum signal to noise ratio and the lowest distortion are obtained when the bandwidth of the system is extremely narrow. Obviously then, the bandwidth of the output of the particle detector must overlap the bandwidth of the electronic system in order to obtain a response. Since the particle flux may be thought of as a periodic driving force, the maximum res-

ponse of the total system is obtained when both the detector and the electronics are tuned to the fundamental frequency of the flux. This suggests that an RF cavity, which produces an output when excited by the electromagnetic field of a charged particle passing through it, be tuned to the fundamental frequency of the flux and be used as the particle detector.

There are several questions which arise in considering the design of such a cavity. First, the geometry and mode of the cavity should be chosen to produce the maximum possible coupling between the charged particle fields and the cavity fields. Second, the material of which the cavity is constructed and its size should be compatible with a high Q factor. Third, a means of detecting the oscillations within the cavity should be chosen which will produce the maximum possible output signal.

The electric and magnetic fields of a moving charged particle have been derived in Reference 21 and can be put in the form:

$$
\begin{aligned}
E_y &= (q\gamma b)/(4\pi\varepsilon_o(b^2 + \gamma^2 v^2 t^2)^{3/2}), \\
E_z &= -(\gamma q v t)/(4\pi\varepsilon_o(b^2 + \gamma^2 v^2 t^2)^{3/2}), \\
B_x &= (\beta/c)E_y, \\
B_y &= B_z = E_x = 0.
\end{aligned}
\qquad \text{(IV-13)}
$$

In these equations the particle passes through the origin of an XYZ coordinate system in the Z direction with velocity v. The fields are given at an observation point b on the Y-axis. The factors β and γ are the usual relativistic parameters and q is the charge of the particle. Equations IV-13 are used to find the field configurations for a charged particle, shown in Figure 20a. Calculations using these equations show that if $\beta \sim .75$, $b \sim .05$ meters, $q = 100e$, then a small wire loop detecting the changing magnetic flux as the particles pass will produce a maximum signal of about 1μvolt.

In general, when a current element is introduced into a resonant cavity all of the resonant modes of oscillation will be excited. For a particular shape and position for the current element the modes which are excited are those which have field configurations most closely resembling the fields of the current element.[25] The cylindrical symmetry of the charged particle fields in Figure 20a suggests that a cylindrical resonant cavity with the cylinder axis coinciding with the particle trajectory would be the optimum configuration for particle detection (Figure 20b). For an axial current element only TM modes can be excited.[25] The simplest TM mode which matches the fields of the charged particles is the TM_{011} mode. This is so because the portion of the standing wave in the cavity which travels to the right in

Figure 20: Field configurations for the resonant cavity particle detector.

a) Electric and magnetic fields in the transverse plane of a moving (out of page) charge.

b) Geometry of cylindrical cavity.

c) Fields of TM_{011} mode in a cylindrical cavity.

a)

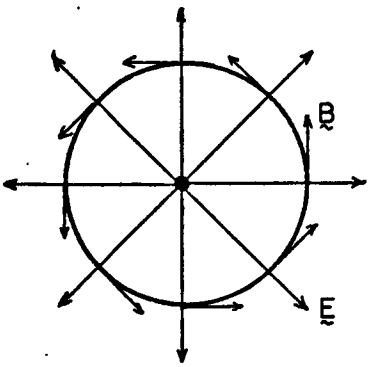

b)

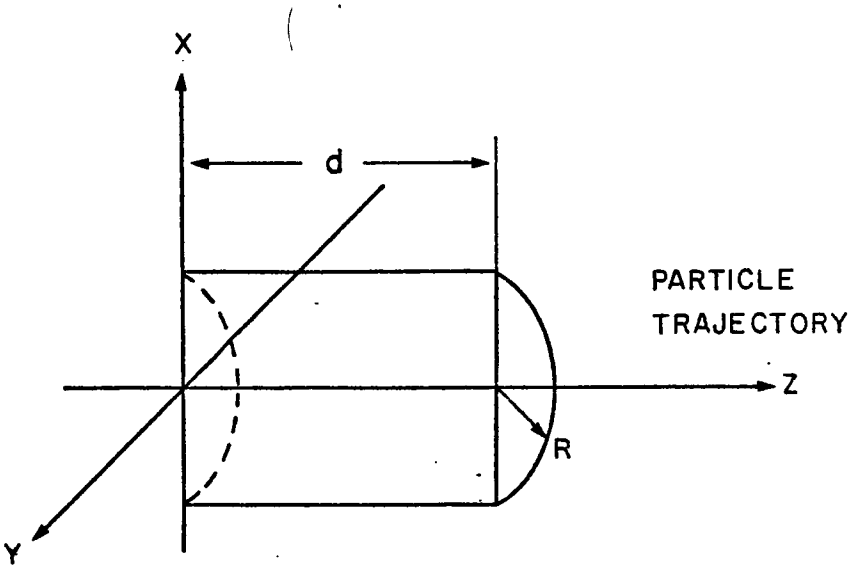

c)

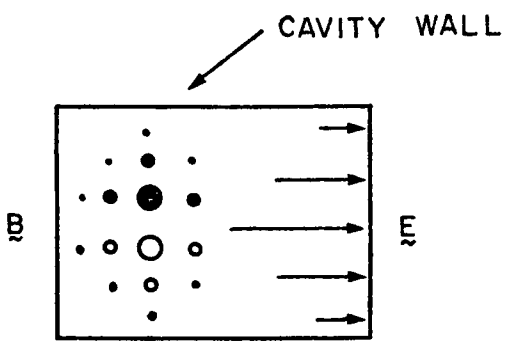

Figure 20b will exactly match the particle's field (Figure 20c). The resonant frequency of a TM_{011} mode is given by:

$$\omega_{011} = c(2.405^2/R^2 + \pi^2/d^2)^{1/2}, \qquad \text{(IV-14)}$$

or for the LAMPF frequency

$$(2.405^2/\pi^2)/R^2 + 1/d^2 = (4/3)^2, \qquad \text{(IV-15)}$$

where R is the radius of the cavity and d is its length. If $d \sim R$ the next lowest resonant frequency is well above ω_{011} [21].

A procedure (not presented here due to its length) for finding the coupling between a resonant cavity mode and the fields of an internal source is explained in Reference 25. Basically, this method involves setting up a time dependent Green's function problem for Maxwell's equations and removing the time variable by using Laplace transforms. Next, the Lorentz reciprocity theorem is used to calculate the Green's function. This involves finding a coupling constant between the TM_{011} electric field and the field of a point current source. After inverting the Laplace transform back to the time variable the excitation due to any current source can be calculated by integrating the product of the source current density and the Green's function over the space and time variables.

For a TM_{011} mode the Q of a resonant cavity is given by:

$$Q = \mu_o/\mu_c \ (d/\delta)1/2 \ (1 + d/2R)^{-1} \qquad \text{(IV-16)}$$

where μ_c is the permeability of the metal and δ is the skin depth.[21] As an example, if d = R = .5meter for a copper cavity at a frequency of 200MHz, then

$$Q \approx 30{,}000. \qquad \text{(IV-17)}$$

The bandwidth of the output of such a cavity is

$$\Delta\omega = \omega_o/Q \approx 4 \times 10^4. \qquad \text{(IV-18)}$$

Several types of RF probes are described in Reference 25. The two most common types are the loop probe, which is sensitive to the magnetic field within the cavity, and the straight probe, which is sensitive to the electric field. The orientation of each type is chosen so that the corresponding field interacts with it as strongly as possible. More detailed calculations have shown that a minimum signal strength of 1μvolt/50 charges can be expected from the entire system. The main advantage of the resonant cavity over the simple wire loop described earlier is its narrow bandwidth. Because of this narrow bandwidth the thermal noise from the cavity will be less than that from the wire loop. Consequently, the resonant cavity should have a much better signal to noise ratio.

V: CONCLUSIONS

A: Theory

In Chapter II, random and periodic particle fluxes were considered as time dependent signals. It was shown that these signals, once measured, could be processed by correlation techniques to produce the TOF spectra of the fluxes. The major results were:

1. Random fluxes
   a. The crosscorrelation of the particle currents measured at two points along the flight path gives the TOF spectrum.
   b. The time resolution of this method will, in general, not be as good as that of particle-by-particle systems if standard particle detectors are used.
   c. Since only particle currents are measured, pile-up problems are eliminated.
2. Periodic fluxes
   a. The crosscorrelation method mentioned above can be used with periodic fluxes only under certain ideal conditions.
   b. If a sync signal is available it can be correlated with the measured particle flux signal to detect the correlation between particle velocity and phase within

the periodic structure.

c. This phase detection method may be applied two different ways.

d. The phase detection methods do not suffer any pile-up problems and offer a possibility of much better time resolution.

3. All particle identification is lost in these current measurements.

These results suggest that for high flux rates correlation detection can be used to avoid pile-up problems. Furthermore, improved time resolution can result from using correlation detection with periodically pulsed fluxes.

B: Experimental

The results of a test at LAMPF of a high speed camera system, which employed a correlation method of section II-C, were reported and discussed in Chapter III. It was found that although the instrument could record the time structure of a pion beam there were many problems with the system which prevented a conclusive decision on its overall ability to significantly improve upon the results of particle-by-particle measurements.

In Chapter IV, a system was proposed which, on paper, should be capable of measuring the TOF spectra of periodic

fluxes with improved time resolution and no pile-up problems. This system uses correlation and radio technology to measure the phases and amplitudes of the velocity components of a flux. The data expected from both of these systems would have to be numerically processed to produce the TOF spectra.

C: Future Endeavors

In order to be a successful system, the Imacon camera needs to be improved in the following areas:

1. Better optical geometry between the particle detector and the image converter tube.

2. Better design of the system to eliminate non-uniformities and provide more useful controls such as a better focusing method and more reliable adjustments of the image converter tube electronics.

Since the system proposed in Chapter IV appears to be capable of better results and is also less costly than the camera, it should be constructed and tested before further efforts are spent on the camera development. This system needs a more thorough analysis of noise effects.

The computational aspects of the data analysis for both systems needs to be more thoroughly considered.

Appendix A: A Review of Signal Theory[10,12]

A signal, s(t), may be defined as "the variation through time of any significant physical quantity occurring in a useful device or system."[16] The function s(t) is called the time domain description of the signal.* The fundamental theorem of signal theory states that an equivalent description of the signal can be given in the frequency domain. This consists of the spectrum of the signal; i.e., a plot of the amplitude and phase of each frequency component of the signal versus frequency. For a periodic signal the two descriptions are related by Fourier series:

$$s(t) = \sum_n S_n e^{jn\omega_o t} \tag{A1}$$

$$S_n = (1/T) \int_{-T/2}^{T/2} s(t) e^{-jn\omega_o t} dt. \tag{A2}$$

For an aperiodic signal, such as a single pulse, Fourier transforms are used:

$$s(t) = (1/2\pi) \int_{-\infty}^{\infty} S(\omega)\ e^{j\omega t} d\omega \tag{A3}$$

$$S(\omega) = \int_{-\infty}^{\infty} s(t) e^{-j\omega t} dt. \tag{A4}$$

Fourier analysis is a linear theory; i.e., the Fourier

*Throughout this paper small letters are used for time domain variables and capital letters for frequency domain variables.

transform (series) of the sum of two or more signals is the sum of the Fourier transforms (series). Additional properties are :

1. For a time delayed signal , $s_d(t) = s(t - t_d)$,

$$S_d(\omega) = [e^{-j\omega t_d}]S(\omega). \tag{A5}$$

2. The transform of $s(at)$ is $(1/a)S(\omega/a)$. (A6)

3. If $f(t) = s_1(t)s_2(t)$ then

$$F(\omega) = (1/2\pi)\int_{-\infty}^{\infty} S_1(u)S_2(\omega - u)du, \tag{A7}$$

and conversely

$$(1/2\pi)\int_{-\infty}^{\infty} S_1(\omega)S_2(\omega)e^{j\omega t}d\omega = \int_{-\infty}^{\infty} s_1(\tau)s_2(t - \tau)d\tau. \tag{A8}$$

The right hand sides of A7 and A8 are called convolution integrals. Similar properties exist for Fourier series.

The bandwidth, $\Delta\omega$, of $s(t)$ is the range of frequency components in its spectrum. The Sampling Theorem states: Any signal which is band-limited to an upper frequency F is completely specified by stating its values at a rate 2F/sec or faster. This is so because the maximum rate of change of a signal is governed by its highest frequency component. The minimum sampling rate is called the Nyquist Rate.

Fourier series or transforms cannot be applied to random signals because the amplitudes and phases of the freq-

uency components are themselves functions of time. However, a different technique, correlation, can be used for an analagous treatment. The correlation, $r_{12}(\tau)$, of two signals is defined as:

$$r_{12}(\tau) = r_{21}(-\tau) = \lim_{T\to\infty} (1/2T) \int_{-T}^{T} s_1(t)s_2(t + \tau)dt. \quad (A9)$$

For example, the correlation function for two statistically independent random functions with zero DC components is $r_{12}(\tau) = 0$. If the two functions are equal aside from the time delay then $r(\tau)$ is called the autocorrelation function:

$$r(\tau) = \lim_{T\to\infty} (1/2T) \int_{-T}^{T} s(t)s(t + \tau)dt. \quad (A10)$$

$r(0)$ is the mean power:

$$r(0) = \lim_{T\to\infty} (1/2T) \int_{-T}^{T} s^2(t)dt. \quad (A11)$$

The spectral density, $P(\omega)$, of a random signal, $s(t)$, is defined as:

$$P(\omega) = \lim_{T\to\infty} (1/2\pi) \overline{\left| \int_{-T}^{T} s(t)e^{-j\omega t}dt \right|^2}. \quad (A12)$$

The Weiner-Khinchin Theorem relates $P(\omega)$ and $r(\tau)$:

$$r(\tau) = 1/2\pi \int_{-\infty}^{\infty} P(\omega)e^{j\omega\tau}d\omega \quad (A13)$$

$$P(\omega) = \int_{-\infty}^{\infty} r(\tau)e^{-j\omega\tau}d\tau. \qquad (A14)$$

Thus, the roles played by $r(\tau)$ and $P(\omega)$ are similar to those of $s(t)$ and $S(\omega)$ for aperiodic signals.

A network or system is any device which produces an output or response, $g(t)$, from an input signal, $s(t)$. A device whose output is $g(t) = g_1(t) + g_2(t)$ for an input of $s(t) = s_1(t) + s_2(t)$ is called a linear system. One property of a linear system is that its response to a sinusoidal signal is a sinusoidal of the same frequency; only the amplitude and phase are changed by the system. For the above two reasons the response of a linear system to a complex signal can be expressed as the sum of the response to each frequency component. Consequently, the transfer function, $H(\omega)$, of a linear system is defined as:

$$g(t) = (1/2\pi)\int_{-\infty}^{\infty} G(\omega)e^{j\omega t}d\omega = (1/2\pi)\int_{-\infty}^{\infty} H(\omega)S(\omega)e^{j\omega t}d\omega, \qquad (A15)$$

$$G(\omega) = H(\omega)S(\omega). \qquad (A16)$$

If $s(t)$ is a unit impulse function then $S(\omega) = 1$. The impulse response, $h(t)$, of the system is given by

$$h(t) = (1/2\pi)\int_{-\infty}^{\infty} H(\omega)e^{j\omega t}d\omega, \qquad (A17)$$

and conversely

$$H(\omega) = \int_{-\infty}^{\infty} h(t)e^{-j\omega t}dt. \tag{A18}$$

So the impulse response and transfer function form a Fourier transform pair and give the time domain and frequency domain descriptions, respectively. Equation A15 may be rewritten as a convolution integral in the time domain:

$$g(t) = \int_{-\infty}^{\infty} h(\tau)s(t - \tau)d\tau. \tag{A19}$$

Since any real physical system has some frequency beyond which its response falls off, an important class of linear systems is the low pass filter. The impulse response of an ideal low pass filter is given below. Assume the transfer function of the filter is given by

$$H(\omega) = \begin{cases} e^{-j\omega t_d}, & \omega \leq \omega_c \\ 0, & \omega > \omega_c \end{cases} \tag{A20}$$

where t_d is the time delay of the response. Using equation A17 gives

$$\begin{aligned} h(t) &= (1/2\pi) \int_{-\omega_c}^{\omega_c} e^{j\omega(t-t_d)}\, d\omega \\ &= (1/\pi)(\sin\omega_c(t-t_d))/(t-t_d). \end{aligned} \tag{A21}$$

See Figure A1. Note that the output pulse has a width $\Delta t \approx 1/2f_c$ and is delayed by t_d.

Many signals have a dependency not only on time, but

Figure A1: The impulse response of an ideal low pass filter.

a) the input function

b) frequency spectrum of the input

c) frequency spectrum of the output

d) impulse response of the filter

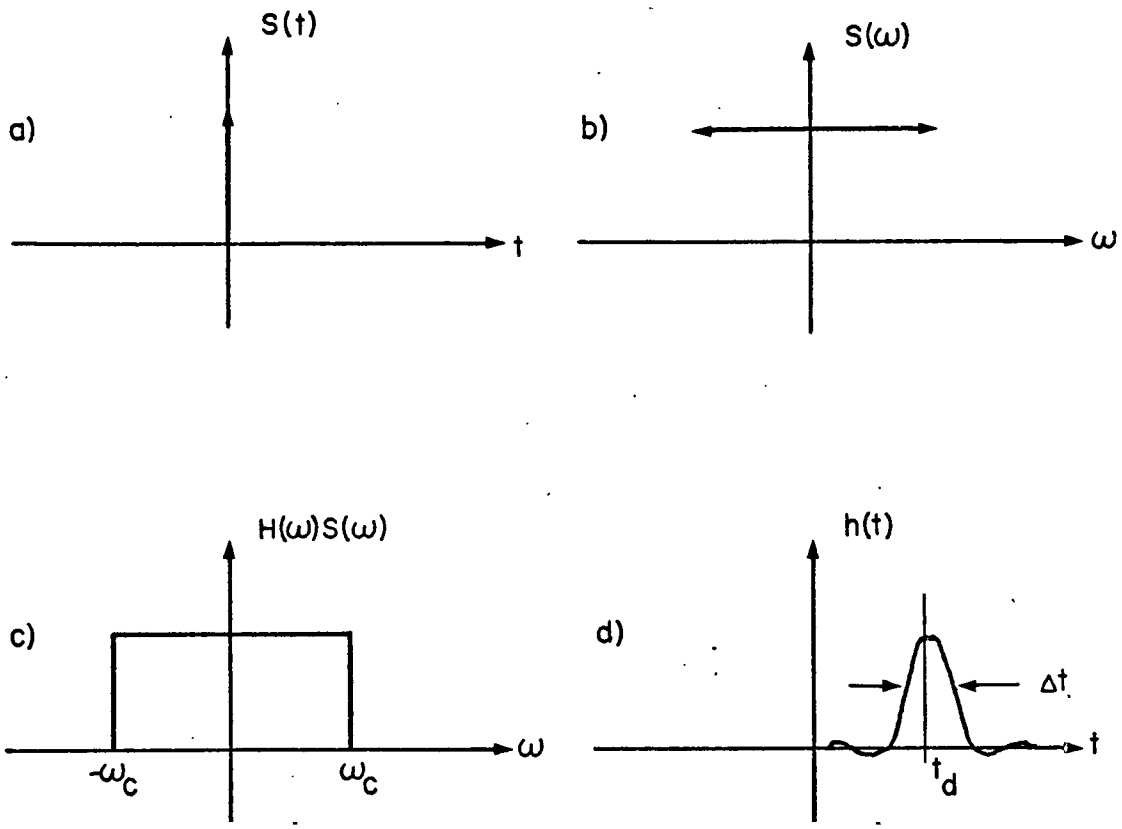
S(t)
a)
t
S(ω)
b)
ω
H(ω)S(ω)
c)
ω
-ω_c
ω_c
h(t)
d)
Δt
t
t_d

also on another variable. For example, the amplitude of electromagnetic radiation from a coherent, monochromatic source varies as $\cos(\omega t - kx)$. The phase of the amplitude depends on kx where $k = \omega/v$ and x is the distance in the direction of propagation. A non-monochromatic source emits radiation of different frequencies. The spectral density, or power spectrum, $G(k)$, of a source can be obtained by a method called Fourier transform spectroscopy. In this method the beam of radiation is split in two and recombined as the path length of one of the meams is varied. The intensity, $I(x)$, is measured as a function of path length difference, x. It can be shown[7] that $I(x)$ is given by:

$$I(x) = \int_0^\infty (1 + \cos kx) G(k)\, dk \qquad \text{(A22)}$$

$$= (1/2) I(0) + 1/2 \int_{-\infty}^{\infty} G(k) e^{ikx} dk.$$

By defining $W(x) = 2I(x) - I(0)$, the following Fourier transform pair is found:

$$W(x) = \int_{-\infty}^{\infty} G(k) e^{jkx} dk$$

$$G(k) = (1/2\pi) \int_{-\infty}^{\infty} W(x) e^{-jkx} dx. \qquad \text{(A23)}$$

Thus, by experimentally measuring the function $W(x)$, the power spectrum, $G(k)$, can be calculated.

Appendix B

The particle flux detection systems considered in section II-C and Chapter IV produce as output the function

$$g(x,\tau) = \sum_v A_v \cos(\omega_o \tau + \theta_v) \tag{B1}$$

where $\theta_v = \omega_o x/v$. This equation can be generalized to continuous velocity destributions:

$$g(x,\tau) = \int_o^\infty A(k)\cos(\omega_o \tau + kx)dk. \tag{B2}$$

Here, $k = x/v$. If $A(k)$ can be calculated using $g(x,\tau)$ then the TOF spectrum is known. This appendix considers the problem of finding $A(k)$ and, in particular, considers the relationship between the velocity resolution and the range of x.

If $\tau = 0$, then equation B2 reduces to

$$g(x) = \int_o^\infty A(k)\cos(kx)dk. \tag{B3}$$

This equation can be inverted by multiplying by $\cos(k'x)$ and integrating over x:

$$A(k') = (1/2\pi) \int_o^\infty g(x)\cos(k'x)dx. \tag{B4}$$

Equations B3 and B4 constitute a Fourier transform pair.

According to equation B4, $A(k')$ can be calculated exactly only if the function $g(x)$ is known for an infinite

range of x values. In an actual experiment the range of x will be limited by the available space along the beam axis and the divergence of the particles in the flux. The effect of a finite upper limit, a, for x is easily derived by considering the case where $g(x) = A\cos(kx)$; i.e., g(x) contains only a single velocity component. Equation B4 becomes

$$A(k') = (1/2\pi)A \int_0^a \cos(kx)\cos(k'x)\,dx$$

$$= (A/2\pi)\sin[a(k - k')]/(k - k'). \qquad (B5)$$

The width of the A(k') distribution if given by

$$\Delta k' \approx \pi/a.$$

Or, in terms of velocity resolution:

$$\Delta\beta \approx (\beta^2\pi/a)(c/\omega_o). \qquad (B6)$$

In order to resolve pions and muons at 250 Mev/c at LAMPF (section I-C) an a of approxomately 10 meters is required. A more careful analysis shows that the muons and pions can actually be resolved for an a value as small as 3-5 meters.

In deriving equation B6 no use of the periodicity of g(x) has been made. If g(x) contains a single velocity component then its period is given by

$$p = 2\pi c\beta/\omega_o = (3/2)\beta \text{ meters}, \qquad (B7)$$

using the ω_o for the LAMPF accelerator. Since the function

repeats indefinitely the upper limit of equation B4 can be extended to infinity once one period of g(x) is measured. In general, the lowest frequency in g(x), which determines the length of a period, is given by $k_{max} - k_{min}$, or

$$p = 2\pi c\beta_{min}\beta_{max}/(\omega_o \Delta\beta). \tag{B8}$$

This result agrees with equation B6 and indicates that in the general case no decrease in the required flight path can be achieved by using the periodicity of g(x).

In certain special cases the TOF spectrum can be found directly from equation B1 by using the ability to vary τ. For example, if a particle flux is known to consist of two velocity components then

$$g(x,\tau) = A_1\cos(\omega_o\tau + k_1x) + A_2\cos(\omega_o\tau + k_2x)$$

or, using phasor notation,

$$g(x,\tau) = A_1 \angle \underline{k_1x} + A_2 \angle \underline{k_2x}. \tag{B9}$$

This equation contains the four unknowns, A_1, A_2, k_1, and k_2 and may be solved by the following procedure. First, a reference phase angle is established by defining $\varphi_o = 0$ when $g(x_o,\tau) = 0$. Next, the amplitude and phase of $g(x,\tau)$ is measured at two more x positions. This will result in the equations

$$B_1 \quad \varphi_1 = A_1 \angle \underline{k_1x_1} + A_2 \angle \underline{k_2x_1}$$

$$B_2 \quad \varphi_2 = A_1 \angle k_1 x_2 + A_2 \angle k_2 x_2. \qquad \text{(B10)}$$

Since each equation contains two measured values they can be solved simultaneously to yield the unknowns. The velocity resolution of this method is limited only by the accuracy with which the amplitudes and phases can be determined.

Appendix C: Čerenkov Detectors[20,21]

Čerenkov radiation is a very weak radiation in the visible region that occurs when a charged particle moves through a dielectric medium with a velocity greater than the phase-velocity of light in that medium. The minimum velocity, $\beta = v/c$, which will produce Č light in a material with index of refraction n is:

$$\beta_{min} = 1/n. \qquad (C1)$$

The Čerenkov radiation does not depend on the atomic number of the medium or upon the mass of the charged particle. Čerenkov radiation may be explained as follows.

The time varying electromagnetic field of the passing charged particle causes polarization of the atoms of the medium by displacing the bound electrons. The excited atoms radiate electromagnetic waves. The intensity of the radiated field at a distant observation point is zero or not zero depending on whether the radiation is emitted coherently or incoherently. The condition for coherence can be obtained from the geometry of Figure C1. In time Δt the charged particle travels distance $\Delta d_p = v\Delta t = \beta c\Delta t$. The emitted light travels distance $\Delta d_1 = (c/n)\Delta t$. A coherent wave front is built up by Huygen's construction at an angle θ

Figure C1: Huygen's construction for Čerenkov radiation. A particle travels distance Δdp during the time, Δt, which the radiation travels distance Δd_1.

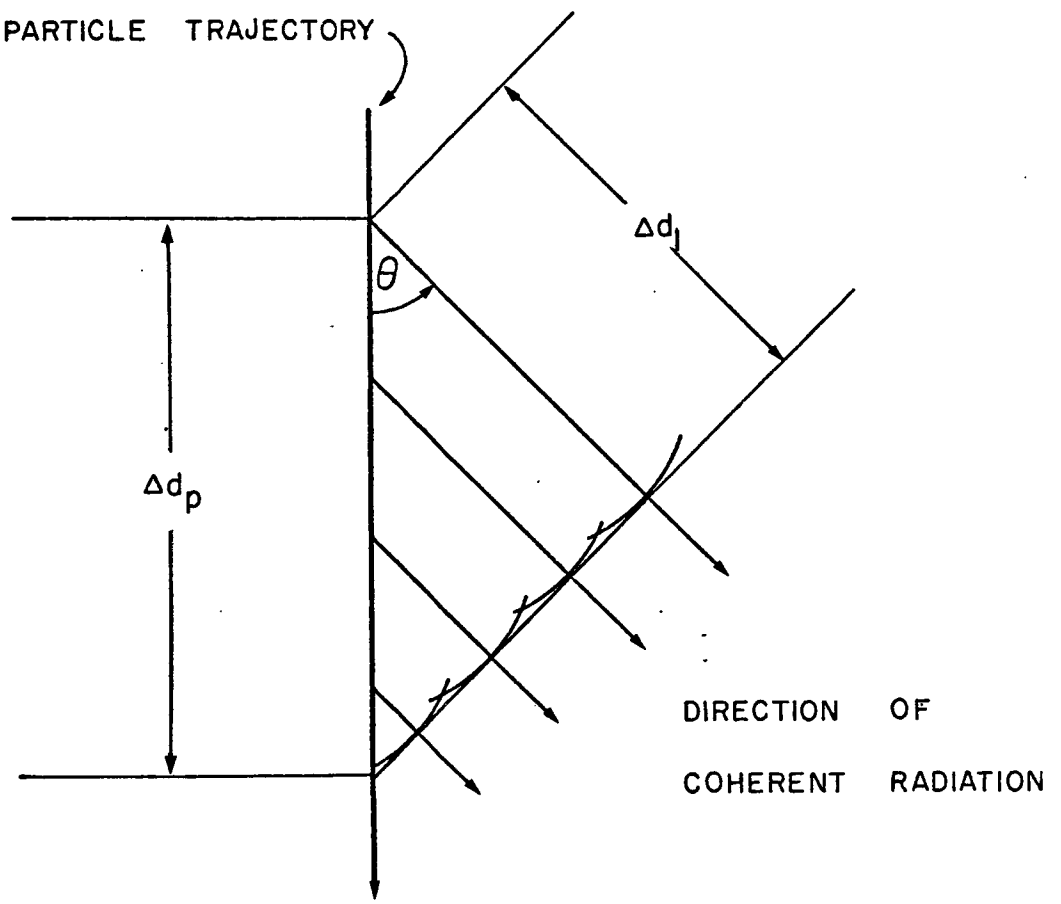
PARTICLE TRAJECTORY
Δd_l
θ
Δd_p
DIRECTION OF
COHERENT RADIATION

such that

$$\cos\theta = \Delta d_1/\Delta d_p = 1/\beta n. \qquad (C2)$$

Thus, the coherently radiated light is emitted in a cone of half angle θ about the axis of the path of the particle. By letting θ approach zero in equation C2, equation C1 is recovered.

Jackson[21] derives a formula for Č light which gives the energy radiated per unit frequency interval per unit path length per particle:

$$dI(\omega)/dx = e^2(\omega/c^2)[1-1/(\beta^2\epsilon(\omega))]. \qquad (C3)$$

By assuming $\epsilon(\omega) \approx n^2$ over the frequency range of interest the formula reduces to:

$$dI(\omega)/dx = e^2(\omega/c^2)\sin^2\theta. \qquad (C4)$$

This formula can be used to predict the number of photons produced as a charged particle passes through a given thickness of material. Note that the number of photons is independent of the velocity of the particle as long as equation C1 is not violated and the particle does not loose a significant amount of energy as it traverses the medium. The number of photons produced per unit frequency per unit length is derived by dividing C4 by $\hbar\omega$, the energy of a single photon.

$$N(\omega,x) = (1/137)\sin^2\theta dx d\omega/c,$$

or

$$N(\omega) = (x/137)\sin^2\theta d\omega/c = (x/137)\sin^2\theta[-d\lambda/\lambda^2]. \quad (C5)$$

$\check{C}$ light is usually detected by a photocathode. The number of photoelectrons produced within the photo tube per $\check{C}$ particle is given by

$$N = (x/137)G(\theta)\sin^2\theta \int_{\lambda_1}^{\lambda_2} -E(\lambda)/\lambda^2 d\lambda. \quad (C6)$$

Here $G(\theta)$ is a geometrical factor which depends on the shape of the Čerenkov radiator and its coupling to the photocathode. The factor $E(\lambda)$ is the efficiency of the photocathode in photoelectrons per photon.

This development only gives an approximate result because factors such as reabsorption of the light by the detector material, loss of light at interfaces, and additional light due to some scintillation have been ignored.

REFERENCES

1. L. V. Coulson et al., Nucl. Instr. and Meth.101,247(1972).

2. P. W. Nicholson, Nuclear Electronics, (Wiley,London,1974).

3. H. Daniel and W. Genter, Methods of Experimental Physics 5B, eds. L. C. L. Yuan and C. S. Wu, (N.Y. Academic Press, New York,1963).

4. Private discussions with members of the Rice University-University of Houston MEP group.

5. L. E. Agnew, LAMPF Users' Handbook, (Informal Report of Los Alamos Scientific Laboratory,1973).

6. E. Dunn, ed., Quaterly Report on the Medium Energy Physics Program, (Progress Report from Los Alamos Scientific Laboratory,1975).

7. G. R. Fowles, Introduction to Modern Optics, (Holt, Rinehart, and Winston, New York,1968).

8. L. A. Wainstein and V. D. Zubakov, Extraction of Signals from Noise, (Prentice-Hall, New Jersey,1962).

9. F. S. Grant and G. F. West, Interpretation Theory in Applied Geophysics, (McGraw-Hill, New York,1965).

10. C. C. Goodyear, Signals and Information, (Butterworth, London,1971).

11. A. M. Rosie, Information and Communication Theory, (Van Nostrand Reinhold, London,1973).

12. P. F. Panter, Modulation, Noise, and Spectral Analysis, (McGraw-Hill, New York,1965).

13. Y. W. Lee, Statistical Theory of Communication, (Wiley, New York,1964).

14. F. Gompf et al., Neutron Inelastic Scattering 2, (IAEA, Vienna,1968)417.

15. G. Wilhelmi et al., Nucl. Instr. and Meth.81,36(1970).

16. J. L. Marshall, Introduction to Signal Theory, (Scranton Penn. International Textbook, Scranton,1965).

17. W. B. Davenport and W. L. Root, An Introduction to the Theory of Random Signals and Noise, (McGraw-Hill, New York,1958).

18. J. F. Colwell et al., Nucl. Instr. and Meth.76,135(1969).

19. Measurements on the Test Channel beam were done by LAMPF personnel D. Werbeck and J. Sherwood.

20. A. P. Arya, Fundamentals of Nuclear Physics, (Allyn and Bacon, Boston,1966).

21. J. D. Jackson, Classical Electrodynamics, (Wiley, New York,1962).

22. Nuclear Enterprises, Inc., Brochure on Plastic Scintillators, Light Pipes, and Čerenkov Detectors.

23. A. B. Cook and A. A. Liff, Frequency Modulation Receivers, (Prentice-Hall, New Jersey,1968).

24. P. R. Bevington, Data Reduction and Error Analysis for the Physical Sciences, (McGraw-Hill, New York,1969).

25. R. E. Collin, Field Theory of Guided Waves, (McGraw-Hill, New York,1960).